Final Technical Report

Report Title:

Establishing the Quantitative Basis for Sufficiency Thresholds and Metrics for Friction Ridge Pattern Detail and the Foundation for a Standard

Award Number:

National Institute of Justice
Award No. 2009-DN-BX-K229

Authors:
Randall S. Murch
A. Lynn Abbott
Edward A. Fox
Michael S. Hsiao
Virginia Tech

and

Bruce Budowle
University of North Texas

May 24, 2012

Abstract

The purpose of this two-year project has been to address the need for a sound, quantitative basis for assessing the quality of fingerprint images. Latent prints, in particular, can be problematic because they are often partial, smudged, and otherwise distorted. Prints of sufficiently high quality routinely allow for *identification* (i.e., originates from one known source) or *exclusion* (i.e., could not have originated from a reference source). However, image quality problems related to identifiable Level 1, 2, or 3 details can be a major source of uncertainty and potential error, or may contribute to a (sometimes incorrect) determination of *no conclusion*. An ability to assess fingerprint image quality therefore represents a crucial step in reaching correct determinations.

The high-level goal of this cross-disciplinary collaboration has been to derive a scientific foundation for measurement of fingerprint image quality, particularly for latent prints. The objectives of this effort have been the following: to make a significant contribution to increasing accuracy, reliability, repeatability, verification, defensibility, and uniform assessment of fingerprint pattern analysis and practice; to provide a demonstrable and defensible basis for engagement of the relevant practitioner and stakeholder communities to incorporate and accept standards into friction ridge pattern analysis, reporting, and use; to provide for substantial improvements to training, proficiency testing, quality assurance, and control (quality management) that are more consistent across the forensic science community; to incorporate metrics that can be documented into the ACE-V or other accepted friction ridge examination methods; to provide the foundation for the development of novel technology aids for human examiners to automate fingerprint pattern image quality determinations; and to provide the basis for image quality determination (accept-reject) that also can be applied with automated fingerprint systems at the point of capture.

The work has been motivated in part by the Daubert ruling (*Daubert v. Merrell Dow Pharmaceuticals*, 1993), as well as by conclusions drawn in the subsequent study by the National Academy of Sciences, *Strengthening Forensic Science in the United States: a Path Forward* (2009). It is reasonable to expect scientific validity when using friction-ridge information for identification or exclusion.

The researchers on this project have followed an experimental approach, testing theoretical concepts through their application to actual images, and then performing statistical validation of the results when possible. Several image databases have been used, containing rolled prints, flat (plain) prints, and latent prints. The researchers also have obtained prints in the laboratory, using latent lifting methods as well as a dedicated live-scan imaging device. Furthermore, the researchers have digitally altered images of actual prints in order to determine drop-off points, that is, thresholds at which an area of friction ridge or feature can no longer be reliably used for identification. Metrics to quantify the effect on image quality have been developed. From these studies, quantitative thresholds have been established for unbiased selection and for use of Level 2 detail, in which both minutia and friction ridges have been incorporated into our formulation.

In conclusion, the results obtained have been noteworthy. First, our hierarchical representation of relations among minutia and friction ridges offers a unique and powerful way for fingerprint search and comparison. In addition, it allows for the mining and detection of unique and rare features that can be extremely useful when drawing statistical likelihood of a given feature. We have also been successful in developing techniques to enhance the accuracy of extraction of ridges and minutia from a print using novel filtering techniques. We developed parallel implementations of our algorithms on a low-cost general purpose graphics processing unit (GPU) and achieved a significant speed-up. Finally, we have successfully created a database of synthetic fingerprints.

Table of Contents

Executive Summary

Fingerprints represent one of the most reliable physiological traits for human identification, and have been widely used for more than a century. In particular, latent fingerprint images obtained from crime scenes have routinely served as crucial evidence in forensic identification. Unfortunately, images of latent prints are often of poor quality, and often represent only a small surface area of a finger's friction-ridge pattern. For a given image, a fingerprint examiner therefore faces the problem of deciding whether friction-ridge details are present in sufficient quantity and quality to proceed with an examination, comparison, and decision. This problem of *sufficiency,* of both quantity and quality of fingerprint image details, has been the focus of this 2-year research project.

The purpose of this two-year project has been to address the need for a sound, quantitative basis for assessing the quality of fingerprint images. Latent prints, in particular, can be problematic because they are often partial, smudged, and otherwise distorted. Prints of sufficiently high quality routinely allow for *identification* (i.e., originates from one known source) or *exclusion* (i.e., could not have originated from a reference source). However, image quality problems related to identifiable Level 1, 2, or 3 details can be a major source of uncertainty and potential error, or may contribute to a (sometimes incorrect) determination of *no conclusion*. An ability to assess fingerprint image quality therefore represents a crucial step in reaching correct determinations.

The high-level goal of this cross-disciplinary collaboration has been to derive a scientific foundation for measurement of fingerprint image quality, particularly for latent prints. The primary objectives of this effort have been the following: to make a significant contribution to increasing accuracy, reliability, repeatability, verification, defensibility, and uniform assessment of fingerprint pattern analysis and practice; to provide a demonstrable and defensible basis for engagement of the relevant practitioner and stakeholder communities to incorporate and accept standards into friction ridge pattern analysis, reporting, and use; to provide for substantial improvements to training, proficiency testing, quality assurance, and control (quality management) that are more consistent across the forensic science community; to incorporate metrics that can be documented into the ACE-V or other accepted friction ridge examination methods; to provide the foundation for the development of novel technology aids for human examiners to automate fingerprint pattern image quality determinations; and to provide the basis for image quality determination (accept-reject) that also can be applied with automated fingerprint systems at the point of capture.

The work has been motivated in part by the Daubert ruling (*Daubert v. Merrell Dow Pharmaceuticals*, 1993), as well as by conclusions drawn in the subsequent study by the National Academy of Sciences, *Strengthening Forensic Science in the United States: a Path Forward* (2009). It is reasonable to expect scientific validity when using friction-ridge information for identification or exclusion.

The researchers on this project have followed an experimental approach, testing theoretical concepts through their application to actual images, and then performing statistical validation of the results when possible. Several image databases have been used, containing rolled prints, flat (plain) prints, and latent prints.

Of particular note is a set of 117,323 anonymized images from 2575 different individuals, which we received on a temporary basis from the FBI's Criminal Justice Information Services division. These were rolled and slap prints, classified as to quality by the FBI as "Good, Bad and Ugly." For latent prints, we relied heavily on the well-known NIST Special Database 27. We also obtained prints in the laboratory, using latent lifting methods as well as a dedicated live-scan imaging device. Furthermore, we have

produced a new database of digitally altered images of actual prints that can be used to determine drop-off points, or thresholds at which an area of friction ridge or feature can no longer be reliably used for identification. Metrics to quantify the effect on image quality have been developed. From these studies, quantitative thresholds have been established for unbiased selection and for use of Level 2 detail, in which both minutia and friction ridges have been incorporated into our formulation.

Our work has been concentrated in four major areas of activity, and this report is subdivided accordingly: 1) feature extraction, 2) quality-based image segmentation, 3) distortion modeling and creation of a fingerprint image database, and 4) high-speed implementation of feature analysis.

In the area of *feature extraction*, we developed our own software for extracting minutiae, ridges, and "extended feature" representations. In addition to extraction of features, we extended them so that they provide quality measures, which we hope will be explored further and serve as a foundation for standardization of latent examination. One avenue of study has led to a technique for improved localization of minutiae, for example, as compared with previous feature-extraction systems. Using 516 fingerprints from NIST SD27, our results exhibited an improvement in minutia accuracy for 88.2% of fingerprint minutia sets after applying the proposed localization method. An increase in average quality of true minutiae was found for 98.6% of the fingerprint images when using a quality assessment technique that we proposed.

In a separate effort, we conducted a form of data mining in order to identify new feature types that are statistically rare. These features are based on hierarchical groupings of minutia triples, or triangles, and are augmented with ridge information. From a relatively small set of 93 images, we found a set of 10 compound features that are statistically unusual, and therefore exhibit high potential for identification or exclusion. An example feature is the following:

> "3 triangles (9 minutiae) such that the total ridge count between all minutia pairs is at least 630, and the ridge count for minutia pairs that lie on different triangles is at least 35."

Our emphasis was not to identify features that are rare for the general population, but instead to develop a procedure for finding such features for any given image database.

Our work in *high-speed computing* was motivated in part by the long computational runs that were required to perform the data mining work. To be valid statistically, exhaustive comparisons are needed for all image pairs in a data set, and the computation time per image pair may be several seconds on a typical modern laptop. This led to mapping of our code from a standard computer to a General Purpose Graphics Processing Unit, often abbreviated as GPGPU or simply GPU. Our implementations have resulted in speedups of 7.6 for single-triangle comparisons and 6.5 for two-triangle comparisons, using a set of 25 images. Our results to date for three-triangle comparisons have shown an average speedup of 12.1 for a set of 6 images. Such performance improvements will be very valuable for data mining on large image databases.

The topic of *image segmentation*, for this project, refers to separation of the foreground (fingerprint region) from the background of an image. Most segmentation of latent prints is performed manually. Traditional automated methods for segmentation are designed for backgrounds with random noise, and they perform poorly on structured/textured backgrounds. The result is that many spurious minutiae are detected by those systems, thus inhibiting the matching process. We developed a novel approach for improving the performance of segmentation in latent prints, with an emphasis on handling structured backgrounds. In our tests, our method reduced the average detected fingerprint area from 60.7% of the total image to 33.6% while maintaining the rate of true minutiae in the fingerprint region. In effect, low-quality portions of the print are being removed from consideration. In a separate test, the rate of true minutiae labeled as background was reduced from 1.4% to 0.3% while maintaining the same average fingerprint region size in comparison to a traditional segmentation method. These results were obtained

using a database of 258 latent fingerprint images from the NIST SD27 database. A segmentation system such as this is potentially a useful aid to human examiners, by directing their efforts to higher-quality portions of an image.

We also have worked on *distortion modeling and creation of a fingerprint image database.* A "foreground" image is produced by applying realistic distortions to any given good-quality fingerprint image. Parameters for these distortions have been chosen by examining databases of good- and poor-quality prints, and by conducting experiments with our live-scan system. Separately, a "background" image is synthesized, to contain random noise and structured noise (lines and text). The background resembles various surfaces on which a latent print can be placed. The foreground image is then merged with the background image to simulate the placement of a finger onto a physical surface.

In conclusion, the results of our two-year research effort have been noteworthy. First, we have developed a novel hierarchical, triplet-based representation among minutiae and associated friction ridges. Such a representation offers a unique and powerful way for fingerprint search and comparison. In addition, it allows for the mining and detection of unique and rare features that can be extremely useful when estimating statistical likelihood of a given print. For instance, we have identified statistically rare features among various prints in a database. Likewise, given a feature, our method also allows for assessing if the feature would be considered rare. We have begun to parallelize the algorithms on a low-cost general purpose graphics processing unit (GPU), and significant speedups have been achieved. By parallelizing the algorithms, we believe much larger databases can be handled. We also have been successful in developing techniques to enhance the accuracy of extraction of ridges and minutia from a print using novel filtering techniques. Finally, we have successfully created databases of synthetic fingerprints. These achievements are aligned with our goals and objectives.

This research has led to several implications for policy and practice. First, our experimental work with databases and with a live-scan system have allowed us to characterize, in part, the large variations in quality that can occur from image capture of friction ridge patterns. Although the statistical work is not yet mature, we believe that this empirical approach will lead to improved guidelines for practitioners. As currently practiced, the interpretation of friction ridge pattern evidence is based primarily on experience, and a large component of the process is subjective. In addition, training can vary substantially from laboratory to laboratory. There is no nationwide standardized education and training curriculum. The differences in training and experience can result in quite varied interpretations of the same evidence by different practitioners, and such differences may impact inculpation and exculpation of suspects and more importantly impinge on the tenet of the presumption of innocence. Confounding the interpretation is a lack of documentation regarding validation of the processes. Validation is essential for determining the limitations of a process or methodology so that practitioners have data to establish guidelines to not exceed the bounds of the system when subjectively interpreting evidence.

The interpretation process also is problematic because the quality of the evidence varies substantially, ranging from highly informative and resolved to partial, smudged, and distorted. Lastly, the quality and quantity criteria for a "print" to meet the sufficiency threshold for interpretation and subsequently for an identification are not defined. Although acceptance of latent print evidence has been accepted in the Courts, legal admissibility is a poor criterion for scientific quality. We all must accept that there are inherent limitations with the current process that need to be improved. These gaps in the system must be addressed.

The studies herein address some aspects of image quality problems related to identifiable Level 1, 2, or 3 details and how such data can be utilized to support the subjective interpretations that to date may not have been validated sufficiently. Moreover, the uncertainty and possibility of error that potentially may

contribute to some practitioners actions to “push the envelope” may soon be able to be quantified so fact finders and triers of fact can be better informed of vagaries, so justice may be better served.

From a policy perspective, our work has laid a foundation for further development, so that sufficiency metric(s) can be developed. Based on our results, however, far more effort is required for development of a more objective support system for interpretation of friction ridge detail. Although more work is needed, the data herein should be considered as part of a more comprehensive training program to promote understanding, increasing accuracy and reliability, and more uniform assessment of fingerprint pattern analysis and practice.

I. Introduction

I.1. Problem statement

Fingerprints represent one of the most reliable physiological traits for human identification, and have been widely used for more than a century. In particular, latent fingerprint images obtained from crime scenes have routinely served as crucial evidence in forensic identification. Unfortunately, images of latent prints are often of poor quality, and may represent only a small surface area of a finger's friction-ridge pattern. For a given image, a fingerprint examiner therefore faces the problem of deciding whether friction-ridge details are present in sufficient quantity and quality to proceed with an examination, comparison, and decision. This problem of *sufficiency,* of both quantity and quality of fingerprint image details, has been the focus of this 2-year research project.

To illustrate the issues that are involved in this research, Figure 1 shows 3 common types of fingerprint images, known as rolled, flat (or plain), and latent prints. The first 2 types are typically obtained from a known individual using ink or a live-scan imaging device, and these prints tend to be of relatively high quality. In contrast, latent prints are often blurred or partial, and may be superimposed onto complex backgrounds as shown in Figure 1(c).

(a) (b) (c)

Figure 1. Sample fingerprint images, all of the same finger. (a) Rolled print. (b) Flat print, also known as a plain print. (c) Latent print.

Today's Automated Fingerprint Identification Systems (AFIS) provide impressive levels of accuracy, but they perform best on high-quality impressions of rolled or flat prints. They operate by extracting features from the images, particularly endings and bifurcations of friction ridges (known collectively as *minutiae*). Identification is performed by computing similarity scores between pairs of images. Because most AFIS implementations are proprietary, algorithmic details are not available in most cases. However, it is clear that they rely heavily on large numbers of minutiae from each print (several dozen, for example).

Latent prints, unfortunately, usually do not allow for extraction of large sets of minutiae. High levels of distortion or noise in the image also may preclude fully automatic analysis. As a result, manual examination typically is required, and additional ridge properties may be needed in order to reach a determination. Several levels of detail (Levels 1, 2, and 3) may be considered in the analysis.

A high-level goal of this project has been to develop objective, scientifically sound criteria that can be used to support the analysis and use of latent prints. When considering a latent print, an examiner tries to make a determination of *identification* (i.e., originates from one known source) or *exclusion* (i.e., could not have originated from a reference source). However, image quality problems can be a major source of uncertainty and error, so in some cases the examiner reaches a decision of *no conclusion*. An examiner

will therefore benefit significantly from clear criteria to indicate that sufficient details are present, in sufficient quality, to proceed with an examination, comparison, and decision.

I.2. Literature citations and review

The term "sufficiency" refers to the quantity and quality (also called "clarity") of information in a friction ridge pattern that is needed in order to proceed with an analysis and render a conclusion. Sufficiency is currently assessed subjectively, according to the training, expertise, and experience of human examiners [1-5]. This step occurs very early in the ACE-V methodology [6]. The "value standard" is also subjective and has no quantitative experimental basis [7]. It is interesting to note that "standards" themselves in this discipline are discussed and formulated in general terms [4, 8] and are not always globally accepted or uniformly applied [9].

Image quality of fingerprints is a major concern in AFIS products. Yet, comprehensive quality control is infeasible because most of the techniques used in those products are proprietary and therefore not available to the broader community for analysis. Studies of fingerprint image quality by NIST have emphasized minutia-based matching systems [10] and include definition of the well-known NIST Fingerprint Image Quality (NFIQ) methodology, which is publicly available. Lee et al. [11] have developed quality index measures specifically for fingerprint images. Similarly, Fierrez-Aguilar et al. [12] have incorporated measures of image quality into automated fingerprint verification systems.

Our early work on friction ridge extraction was heavily influenced by the work described in [13], in which grayscale information was used to trace ridges. Refinements were described in [14, 15]. The use of ridge information for matching in automated systems is starting to attract attention [16-18], but with varied success. The common theme to all previous attempts is that they rely on binary skeleton images, rather than on grayscale, as described in this report.

Our approach to minutia distributions initially bears similarity to work described in [19-24]. A major difference, however, is our incorporation of information from ridges, particularly the ridge direction at each minutia. In fact, the use of extended features for fingerprint analysis has been gaining interest in the automated ten-print community [25]. As noted in [26], additional features are needed for effective processing of latent images. A memo released by the Scientific Working Group on Fingerprint Ridge Analysis, Study, and Technology (SWGFAST) [27] points to the use of "ridges in sequence" by experienced latent examiners, representing important information that is ignored by current AFIS techniques.

Distortion is also an important aspect of fingerprint image analysis. Cappelli and Maltoni [28] developed a model of elastic skin deformation. Ross et al.[29] proposed a deformable thin-spline model to improve the fingerprint matching. Watson et al. [30] designed distortion-tolerant filters to match elastic-distorted fingerprints. All of these are 2-D models.

I.3. Rationale for the research

Fingerprint information has been used for law enforcement purposes since at least 1893, when the Home Ministry Office of the United Kingdom accepted the premise that no two individuals have the same friction-ridge patterns [31]. For more than a century, the testimony of human examiners has been used to identify (or exclude) individuals based on fingerprint evidence. In 1993, however, the U.S. Supreme Court ruled (in *Daubert v. Merrell Dow Pharmaceuticals*) that a scientific basis is needed for expert testimony. The high-level goal of this project has been to develop a scientific foundation for measurement of fingerprint image quality, so that a human examiner will be assured that the quality is sufficient to proceed with an examination, comparison, and decision.

I.4. Personnel

Several graduate students contributed extensively to the success of this project. A partial list follows, shown alphabetically: Kelson Gent, Kevin Hoyle, Nadia Kozievitch, Jonathan Leidig, Lin Tzy Li, Supratik Misra, Sung Hee Park, Indira Priyadarshini, and Nathan Short. Undergraduates who participated are Shubhangi Deshpande and Sony Vijay. The Principal Investigators gratefully acknowledge their hard work.

II. Methods

This section describes our work in the areas of 1) feature extraction, 2) quality-based image segmentation, 3) distortion modeling and creation of a fingerprint image database, and 4) high-speed implementation of feature analysis.

II.1. Feature extraction and analysis

Our research has emphasized several aspects of feature extraction related to fingerprint images. The areas of emphasis have been ridge extraction, minutia localization, minutia quality assessment, and extended feature sets based on minutia triplets. Each is discussed separately in this section.

Ridge extraction. We developed new approaches to extract individual friction ridges from grayscale images. Most published methods for this problem rely on binarized images, in which every pixel is either completely black or completely white. Our approach, however, analyzes grayscale images directly because of the stronger potential to perform quality assessment. For a typical grayscale image, every pixel is represented by a brightness (intensity) value in the range from 0 to 255.

Our approach uses Bayesian techniques to extract ridges [32], motivated by the work of Maio and Maltoni [13] and Liu, Huang, and Chan [33]. As illustrated in Figure 2, the algorithm assumes that ridges are represented as a set of local maxima in image *I*, where higher intensity values represent darker shades of gray. For a given point in *I*, the ridge direction is assumed to be perpendicular to the intensity gradient. For efficiency of implementation, a directional flow map based on intensity gradients is computed in advance. The algorithm makes a sequence of steps along each ridge of interest, using the directional flow map and a user defined step size of several pixels. At each step, the center of the ridge is determined by searching for a local maximum in the direction orthogonal to the current ridge direction. To reduce susceptibility to noise, Gaussian smoothing and regularization are applied to a linear cross-sectional strip that cuts across the ridge.

A problem with previous approaches is illustrated in Figure 3, in which a ridge ending is not detected. We found that neither of the previous algorithms ([13] and [33]) is well equipped to extract ridge segments when bifurcations are present. To address this problem, we introduced new criteria for improved minutia detection, with the result that ridges are extracted more accurately. We developed a Bayesian approach to identifying ridge and valley crossings, using feature vectors of the form $\hat{f} = [\bar{\theta}, \quad \lambda, \quad \psi]$, where $\bar{\theta}$ represents the average direction of intensity gradient for a given image window, λ is the length of the window, and ψ is an adaptive term that is related to the variance of pixel values within the window. Wider (and therefore larger) windows tend to reduce sensitivity to noise, but at the expense of accuracy for narrow ridges and valleys.

In order to implement the classifier, distribution models were needed for each of the three feature types. We obtained the distribution models through parameter estimation using a set of training samples. The training samples were collected from several images by manually selecting points near the centers of ridge sections. For each selected point, a data collection system then automatically captured several nearby image windows that served as representative cases that a ridge crossing is (or is not) present.

Experimental results are given in Section III.1. More technical details are provided in [32].

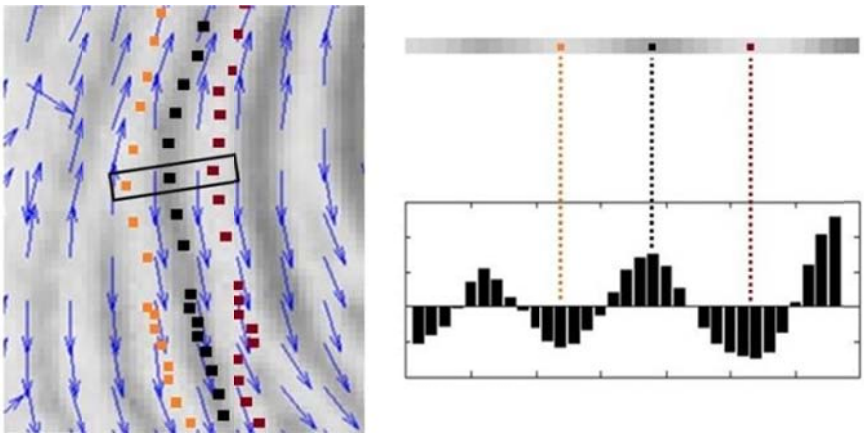

(a) (b)

Figure 2: Illustration of ridge following using the Bayesian approach. (a) Ridge points are indicated (black), along with left and right valley points (orange and maroon, respectively). A group of 3 such points, as shown in the rectangle, is used along with intensity gradient direction (blue) to select the next ridge point. (b) Intensity values are shown for the orthogonal cross section indicated by the rectangle in (a). The local maximum near the center is the ridge point, and it is flanked by local minima indicating the valleys.

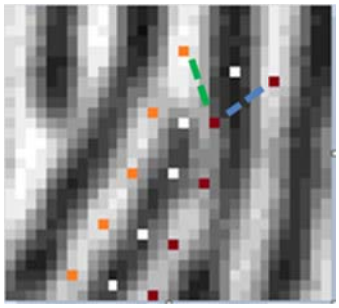

Figure 3: Example of ridge jumping. Previous techniques ([13] and [33]) failed to detect the ridge ending that appears near the center of this image.

Minutia extraction and localization. We developed a novel method for refining estimates of minutia positions from existing minutiae for improved performance and interoperability among feature extractors. Figure 4 provides an overview of the localization procedure. After initial detection of minutiae, the location estimate of each is refined by 1) generating an idealized grayscale template for the neighborhood of that point, and 2) conducting a correlation-type search in the grayscale image using that template. The goodness of fit is then used to compute a quality score for that minutia. A strength of this approach is that templates are not predefined, but are tailored to the locally observed ridge structure.

In our implementation, a ridge skeleton is generated by binarizing and thinning a given grayscale image. This method was chosen over the method proposed for extraction in II.1 due to its low time complexity. The grayscale image and its skeleton are then used to produce an idealized grayscale template near a given minutia point. The resulting template is a representation of the minutia region based on the local structure.

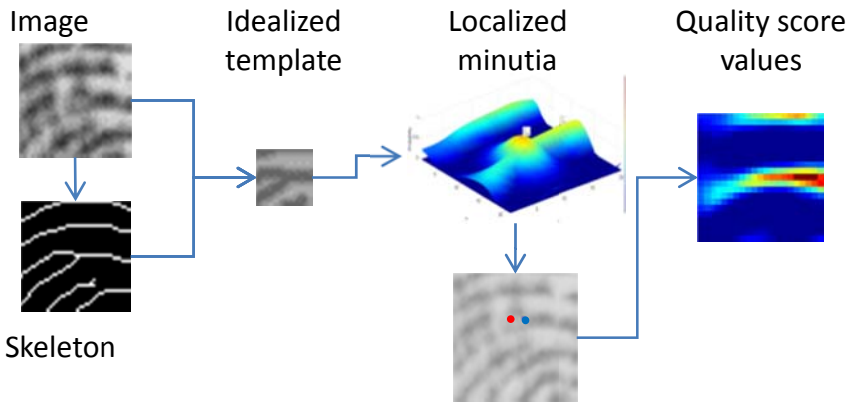

Figure 4: Minutia localization procedure. An image and its skeleton are analyzed to extract an idealized representation of the minutia region.

Our template is generated using $T'_{i,j} = -\cos(2\pi f d_{i,j})$, where f is the local ridge frequency estimated using the approach of [34], and $d_{i,j}$ is the Euclidean distance in the image from pixel (i, j) to the nearest ridge point. The template values $T' \in [-1, 1]$ are calculated for every point inside a small region of interest centered on the candidate minutia. The model assumes that extrema of $T' = -1$ occur at ridgelines, and extrema of $T' = 1$ correspond to valley centers. For computational efficiency, values for distance d can be computed in advance for a skeleton of interest using the distance transform proposed by [35]. This template is adjusted to local image contrast using $T_{i,j} = \sigma_{ROI} \cdot T'_{i,j} + \mu_{ROI}$, where σ_{ROI} is the standard deviation of intensities within the small region of interest, and μ_{ROI} is the mean intensity within the same region. The result is a template that is adapted to the region surrounding the proposed minutia point, with $-r_x \leq i \leq r_x$, $-r_y \leq j \leq r_y$, and r_x and r_y defining the size of the neighborhood.

An example of an observed minutia region and a synthesized minutia template is shown in Figure 5. Parts (a) and (b) of the figure show the original image neighborhood and the corresponding skeleton, respectively, both centered on a bifurcation. The generated template is shown in Figure 5(c). Parts (d) and (e) show 3-D plots of grayscale values for the original image and for the template, respectively. Notice that the ridgelines in the template are essentially uniform in height, unlike those in the original image.

Our approach to localizing minutia is a novel application of particle filters, which are typically used for approximating unknown distributions in probabilistic tracking. Our implementation is based on the CONDENSATION algorithm by Blake and Isard [36]. It consists of iteratively estimating the target state distribution by random sampling and updating the posterior density based on new observations. Instead of assuming that the type of distribution is known (e.g., normal), the conditional state density is represented as a set of weighted samples. The conditional state density $p(s_t|o_t)$ represents the probability of the state (s_t) given the observation (o_t) at time t.

The method introduced here adapts the notion of tracking over time to iterative refinement of minutia location within a static image. The location of a minutia point s_t (at iteration step t) is used as the target state, and the image region of interest o_t is used as the observation. The location estimate is updated using

$$E[s_{t+1}|o_t] = \frac{\sum \omega_t s_t}{\sum \omega_t}, \quad (1)$$

where ω_t is the set of sample weights and s_t is the set of samples at iteration *t*. First, a set of *N* sample points, s_0, is initialized by choosing the points corresponding to the highest cross-correlation scores. Then from sample set s_{t-1} a set of expectation points, ε, are found by randomly generating points (normally distributed) around their respective sample point, $s_i \in s_{t-1}$.

A Gaussian density function is found that is oriented along the local ridge flow direction. The ridge flow direction and the direction reliability maps are found similarly to the method proposed by Jain, Hong, and Bolle [37]. Now we can determine the new set of sample points, $s_i \in s_t$ using

$$s_i = \frac{\sum p(\varepsilon^k)\, \varepsilon^k}{\sum p(\varepsilon^k)}. \tag{2}$$

Weights are assigned to the samples based on the cross-correlation response of template matching at each sample point. This yields a set of sample weights ω_t at iteration *t*. Finally, the expected minutia point at iteration *t*+1 is found using (1). The process is repeated until the filter converges or until the number of iterations reaches a predetermined limit. In order to avoid the problem of degeneracy, where one particle begins to dominate the others due to varying weights, a Sampling Importance Resampling (SIR) particle filter is used, as described by Arulampalam et al. [38]. The resampling algorithm will remove sample points that have small weights, relative to the set, and replace them with other samples in the set.

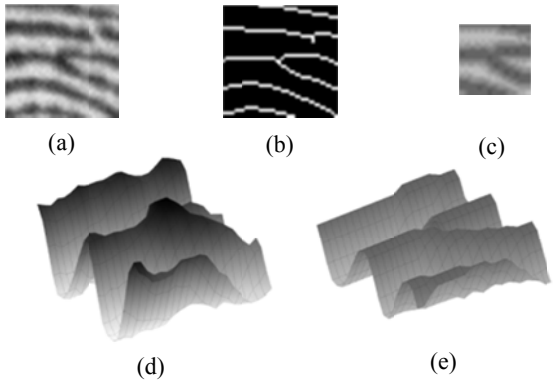

Figure 5: Region of interest centered on a bifurcation in (a) a grayscale image and (b) the corresponding ridge skeleton image. (c) Ideal template generated from proposed method. For comparison, 3-D renderings are shown for (d) the original image region and (e) the idealized template.

Experimental results are given in Section III.1. More technical details are provided in [39].

Minutia quality assessment. Our system assigns a minutia quality value in a manner that is similar to one described by Watson et al. [40]:

$$Q_m = \begin{cases} 0.50\, I + 0.49\, R & if\ L = 4 \\ 0.25\, I + 0.24\, R & if\ L = 3 \\ 0.10\, I + 0.14\, R & if\ L = 2 \\ 0.05\, I + 0.04\, R & if\ L = 1 \\ 0.01\, I\, R & if\ L = 0 \end{cases} \tag{3}$$

The value L is the quality level from the block associated with the localized minutia, and is found using a method similar to that of Ratha, Chen, and Jain [41]. The minutia reliability measure R is taken from a computed cross-correlation value, using a minimum of 0 to avoid negative values. Finally, I is taken from the number of iterations that were required for the particle filter to converge on a minutia point. Specifically, $I = \frac{N_c - 3}{MAX}$, where N_c is the number of iterations until convergence and MAX=10 is the maximum allowable number of iterations. It follows that I is equal to 1 for fast convergence (3 iterations) and 0 for slow convergence (10 iterations). The idea is that a slower convergence will result from a large variance in location of large correlation scores throughout the region of interest. It is expected that a high quality region would provide a large correlation density around a single point.

Experimental results are given in Section III.1. More technical details are provided in [39].

Extended feature sets. Most fingerprint matching systems rely primarily on minutiae, which are the endings and bifurcations of friction ridges. Minutia-based descriptors are used to compare a probe print to a known exemplar. As the surface area of the fingerprint decreases, such as in latent prints, the number of minutiae also decreases, leading to lower identification performance. To overcome this problem, "extended feature sets" have been proposed to make up for the reduced number of minutiae.

Here, we introduce an additional feature called a *ridge component*, which is the portion of a friction ridge that joins two adjacent minutiae on that ridge. In our implementation, each minutia is assigned an additional set of descriptors indicating the ridge components that are directly connected to it. It follows that a termination will have exactly one ridge component descriptor, and a bifurcation will have three.

A *ridge connection* is a binary indicator between two minutiae; it is true if the minutiae share a common ridge component, and it is false otherwise. Using this notion of ridge connections, it is possible to create a graph-based representation of the fingerprint, where each minutia represents a node in the graph and a ridge connection indicator determines if an edge exists between each node. Looking at all possible sub-graphs, the ridge clusters, or groups, can be defined by the set of nodes in which there exists a path from each node to every other node. This set of definitions is illustrated in Figure 6.

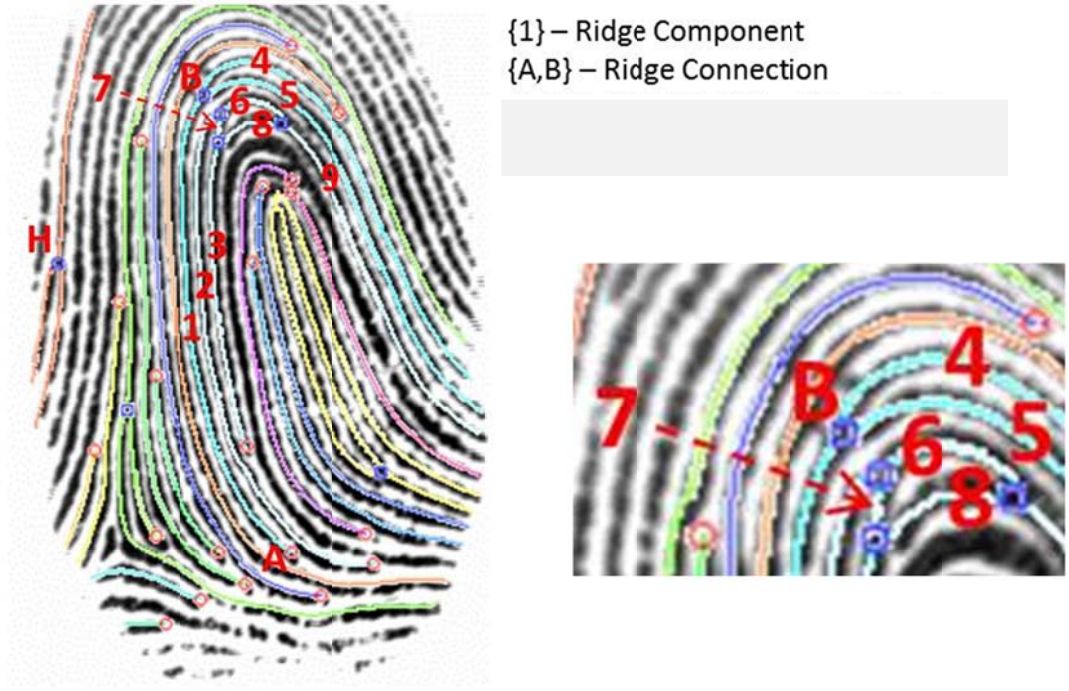

(a) (b)

Figure 6: Fingerprint image with extracted ridge components and minutiae overlain to illustrate several definitions. (a) Complete fingerprint. (b) Enlargement near minutia B. Ridge component 1 joins minutiae A and B. Minutia B is a bifurcation, and is also connected to ridge components 4 and 5. These three ridge components form a single ridge cluster.

Minutia triplets and rarity. Latent fingerprint examiners often search for attributes of a print that are unusual, and therefore especially valuable in reaching identification/exclusion decisions. A major theme of this project has been a search for fingerprint image feature types that have the potential to be highly discriminatory. By identifying and quantifying distinctive features, we can begin to achieve multiple goals: 1) to solidify the scientific foundation for assessment of quality, or lack thereof, for latent fingerprint images; 2) to develop a more complete set of features from which to select descriptors; and 3) to develop objective metrics to determine the extent to which a given latent print is of sufficient quality to proceed with an examination, comparison, and identification or exclusion. More generally, a goal has been to perform data mining in order to identify spatial distributions of minutiae and ridges that are statistically rare.

We have addressed these objectives using features based on 3-point sets of minutiae, which we refer to as triplets or triangles. The resulting extended feature sets are hierarchical, consisting of 2 or 3 minutia triplets together with ridge information. Minutiae are often extracted and represented in "template" form as *xyt* values, where *x* and *y* refer to the (*x*, *y*) coordinates of a minutia within the image, and *t* represents theta, the direction of the ridge that is associated with the minutia.

Any combination of three minutiae can be viewed as the vertices of a triangle. The attributes we used are 1) side lengths of the triangle, or pairwise distances between minutiae; 2) ridge count, or number of ridges crossed, between pairs of minutiae; and 3) whether each pair of minutiae shares a ridge component. Figure 7 shows a minutia triangle and its associated attributes. We also choose to restrict the length of each side to a maximum threshold value in order to keep the triangle as a localized feature, thus reducing the effect of possible skin distortion that becomes more pronounced over longer distances in the image.

One of the main benefits to this descriptor type is that it is rotation- and translation-invariant. This may play an important role when analyzing latent prints, which are less likely than rolled or flat prints to be of a known orientation.

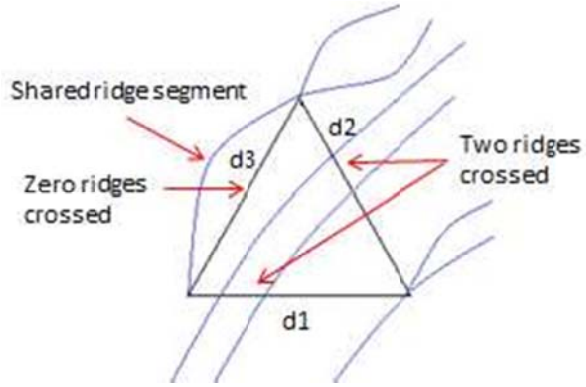

Figure 7: Example triangle-based descriptor. Each vertex represents a minutia point. Also shown are a shared-ridge segment, ridge counts, and side lengths d1, d2, and d3.

We extended the concept of a single triangle to groups of 2 or 3 triangles (containing up to 6 or 9 minutiae). By extending the feature size in this way, while still using the triangle as a foundation, we achieve benefits of modularity and hierarchy that enhance discriminatory power without significantly greater computational cost.

When we consider multi-triangle features, a new set of attributes to consider opens up: those of inter-triangle relations. Figure 8 illustrates a multi-triangle example. Specifically, we consider the ridge count between pairwise minutiae between two different triangles (inter-triangle ridge count), and also look for shared-ridge segments between minutiae of different triangles (inter-triangle shared-ridge segments). As we analyze a latent image containing 6 or more minutiae, such multi-triangle features may potentially provide immense value when comparing against a set of ten-print images of suspects. One could first check if any ten-print image contains similar multi-triangle features. However, the confidence in the match may not be too high if the multi-triangle feature can be found in many other fingerprints. Stated differently, the confidence would be increased if the matched multi-triangle feature from the latent is rare, that is, the feature occurs very infrequently in the population.

In our data mining study, we identified a set of features that were observed to occur infrequently (only one occurrence within our database). The usefulness of such features can then be tested. First, using only the minutiae involved in the feature, we perform a standard minutiae matching algorithm on a small database of fingerprints. Either a set of matches is returned or a ranking score for the most similar fingerprints is returned. Second, we match with knowledge of the distinctiveness of the feature, i.e., we check if that feature exists in the database. Ideally that feature will only be found on a fingerprint that is a true match.

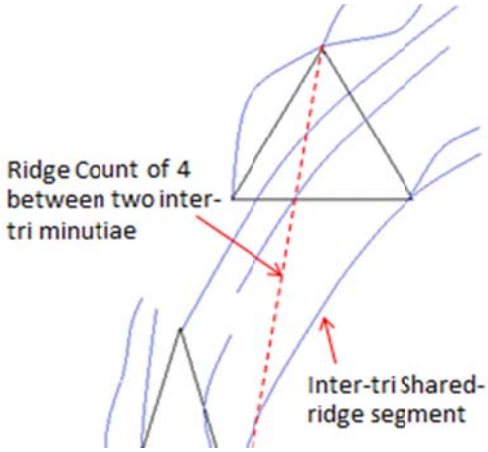

Figure 8: A 2-triangle feature with an inter-triangle shared-ridge and inter-triangle ridge count indicated.

We profiled our fingerprint database to get an idea of what might constitute "rare". Examples of triangle-based feature types that resulted are sum of triangle side lengths, longest side length, shortest side length, sum of ridge counts, number of shared-ridge segments within the triangle (0-3 possible), and length of those shared-ridge segments. We can then see that, for example (with maximum side length restricted to 150 pixels), only 0.065% of triangles have a ridge count > 45 (sample size: 44 fingerprints). This type of information will be useful later to combine different parameters to find distinctive spatial distributions of minutiae.

To discover distinctive spatial distributions of minutiae, the algorithm can be divided into a two-part process. In part 1, all triangles (restricted to some maximum side length) in the fingerprint are processed. Only triangles that are interesting in some way are kept. By "interesting," we mean those that have potential to contribute to a distinctive feature. Examples are triangles with a high ratio of ridge count to side length, or triangles with one or more shared-ridge segments. In part 2 of the algorithm, all of the triangles from the previous step are processed and formed into 2-triangle or 3-triangle groups. Again, we have a list of parameters that we can adjust in order to find distinctive features. For example, we might look for all 3-triangle features where each of the triangles has at least one shared ridge segment, *and* there is also a shared-ridge segment between each of the triangles, *and* on each of those inter-triangle shared-ridge segments the ridge count is at least some minimum value *w* (see Figure 8).

The method for finding such distinctive features involves tuning the parameters such that the feature is unique within a given database. Consider the following example: parameters are selected which yield 5 occurrences of a given feature. Then, we further restrict the parameters, and observe that 0 occurrences are found. So we slightly relax a parameter until 1 occurrence of the feature is found. Then for the given database, this particular feature is very rare and therefore has high discriminatory power. An important aspect of this approach is that any given database can be mined in this way to find features that are statistically rare for that particular database, using an arbitrary set of feature-extraction tools. We believe this approach could be applied to very large fingerprint databases, by researchers with access to such.

Experimental results are given in Section III.1. More technical details are provided in [42].

II.2. Quality assessment and segmentation of latent fingerprint images

A problem area of fundamental importance for latent fingerprint images is the segmentation of those images. As the term is used here, segmentation refers to the identification of image portions that contain friction ridge information. Essentially, the problem can be viewed as one of distinguishing friction-ridge "foreground" from an arbitrary "background." Traditional methods that are used to segment plain prints often fail when the background noise is highly structured, as is common in latent images. Additional complexity arises when a single latent image contains multiple overlapping fingerprints.

We have developed a novel approach to segmenting the fingerprint region from the background in a latent image. Such a capability has the potential to reduce the amount of time spent by a latent examiner, and also may reduce the number of false minutiae that are extracted by automated systems by more accurately defining the fingerprint region. The segmentation method presented here is invariant to fingerprint orientation and, in some cases, can distinguish multiple prints appearing in an image. The method is able to reduce the detected fingerprint area while also reducing the number of minutiae falsely labeled as part of the background.

The proposed algorithm approaches the problem of latent fingerprint segmentation from the perspective of a human examiner by searching for regions in the image that have appearance and structure similar to typical friction ridges. The algorithm generates an "ideal" ridge template and uses it to determine "goodness of fit" scores for local regions of the fingerprint image. Threshold levels can be set to specify different levels of quality in the image, and to distinguish foreground from background. In addition, a Hough-based method is proposed for identifying straight lines in the image and correcting the errors introduced by the lines during ridge flow computation. This is motivated by the fact that lines can fool automated systems because they exhibit properties similar to those of friction ridges and the error in ridge flow direction caused by the lines can affect the match score when utilized in latent print matching, such as in [26]. Figure 9 shows a workflow diagram outlining the proposed segmentation method aimed at detecting background regions with structured noise. This approach can detect any number of lines within the fingerprint image of any size or orientation, however; false positives do arise within the fingerprint region because of the continuous nature of the ridges. Because of this, constraints on the minimum length of a line and maximum distance between segments must be met. These values were determined from a trade-off between genuine and falsely detected lines from a set of test images.

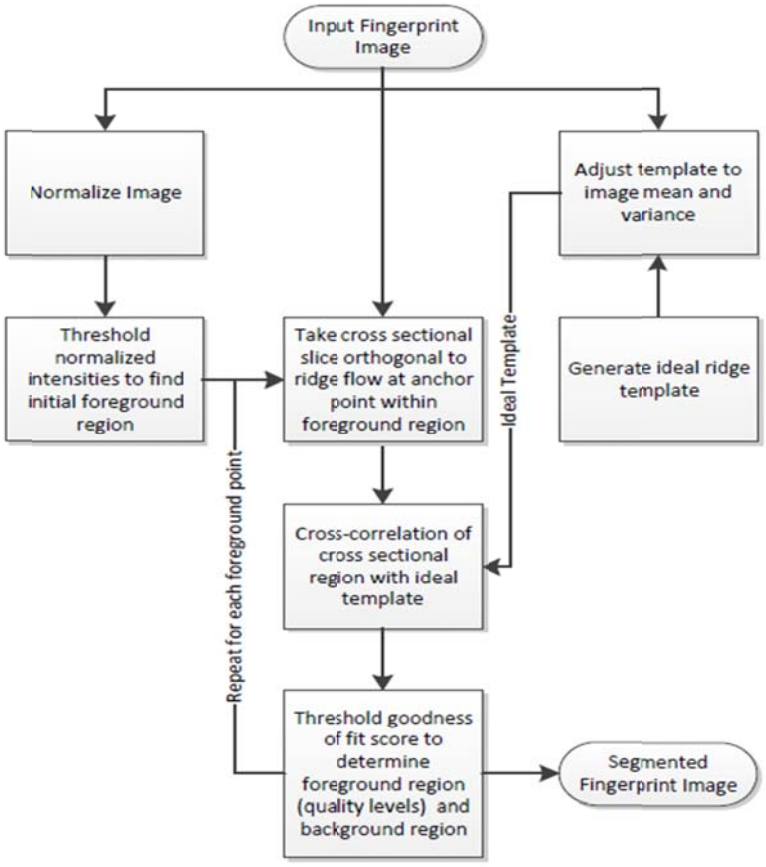

Figure 9: Work flow for proposed segmentation method.

The segmentation steps depend in part on techniques introduced in the earlier section on *Minutia extraction and localization.*

In order to locate and assess ridges in the image, we again use the template model $T'_{i,j} = -\cos\left(2\pi f d_{i,j}\right)$, which was introduced on page 12 of this report. For this problem we set f to the value 1/9 empirically, because average separation between ridge peaks is approximately 9 pixels in a 500 dpi image. Using this fixed ridge frequency, the local ridge quality score is affected by varying ridge frequency due to skin distortion. The ridge flow direction is computed as the angle orthogonal to the intensity gradient and median filtering is applied to reduce the effects of noise. The system adjusts for local image contrast, as described earlier. An example of an observed ridge cross section is shown in Figure 10(a). Parts (b) and (c) of the figure show the original image neighborhood of one of the peaks of the cross section and of the corresponding generated template. Parts (d) and (e) show 3-D representations of the observed ridge segment and generated template. Notice that the ridgelines in the template are essentially uniform in height, unlike those in the original image.

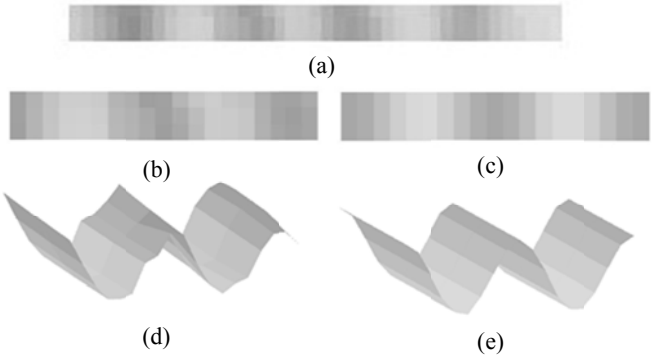

Figure 10: Illustration of idealized ridge templates. (a) Example cross section of ridge surface, with 4 ridges appearing as dark pixels. (b) A subset of the cross section centered at one of the peaks. (c) The ideal sinusoidal template that was generated for (b). (d)-(e) 3-D renderings of (b) and (c), respectively.

A local quality score is assigned using the following cross-correlation,

$$C_s = \frac{\sum_{i,j}\left(T_{i,j}\right)\left(I_{(x+i),(y+j)}\right)}{\sqrt{\sum_{i,j}\left(T_{i,j}\right)^2 \sum_{i,j}\left(I_{(x+i),(y+j)}\right)^2}}, \tag{4}$$

where T is the template image and I is the local fingerprint image within the region overlapped by the template $T_{i,j}$ centered on the image I at location (x, y). The scores in (5) are normalized, so that a value of 1 indicates a very good match of the template to the original image. A value of 0 indicates no correlation, and -1 indicates inverse correlation. The cross-correlation score is used in conjunction with threshold levels to separate foreground from background and to determine quality level, Q_s, of the regions. We have empirically chosen the following levels for determining quality:

$$\begin{cases} Level\ 5 & 0.6 < C_s \leq 1.0 \\ Level\ 4 & 0.4 < C_s \leq 0.6 \\ Level\ 3 & 0.3 < C_s \leq 0.4 \\ Level\ 2 & 0.2 < C_s \leq 0.3 \\ Level\ 1 & 0.1 < C_s \leq 0.2 \\ Level\ 0 & otherwise \end{cases} \tag{5}$$

The foreground blocks are Levels 1-5 and the background is labeled as Level 0. The quality breakdown is described here: 5) Excellent, 4) Good, 3) Medium, 2) Poor and 1) Bad.

Experimental results are given in Section III.2. More technical details are provided in [39].

II.3. Distortion modeling and creation of a synthetic image database

We have investigated models of skin elasticity, and we empirically tested a model that is based on the work of Miao and Maltoni [13]. As illustrated in Figure 11, if a finger is pressed against a planar surface and then dragged or rotated slightly, this model assumes that a central portion of the skin will remain fixed, while the outer portion undergoes rigid translation and/or rotation. Between the inner and outer rigid parts of the skin lies a small area of skin that exhibits elastic deformation.

We developed an interactive software tool known as *fpCreator* that applies this distortion model to any given fingerprint image. In addition to these geometric transformations, the tool also can introduce noise,

add directional blurring, and cause arbitrary dropouts from the image. Figure 12 compares results from the simulator with actual images that we have obtained from a livescan system.

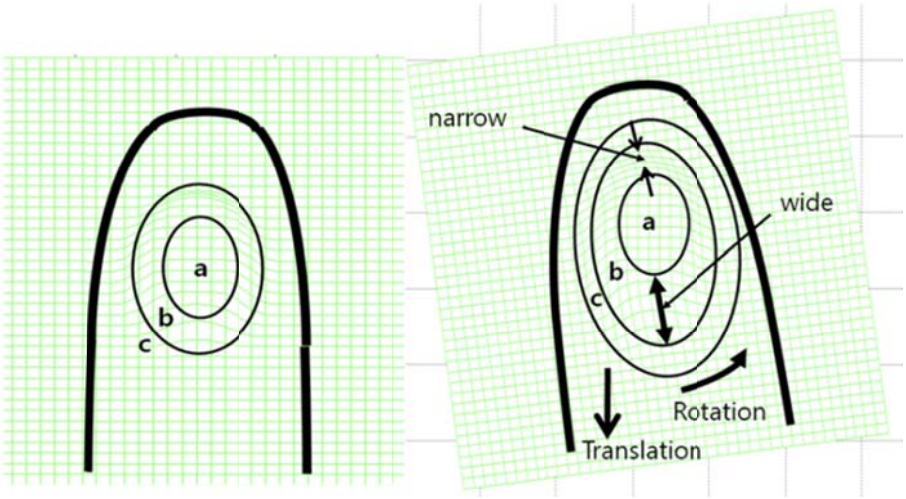

Figure 11: Illustration of geometric skin distortion model. The center ellipse (a) remains rigid as the rest of the finger rotates. The skin region labeled (b) undergoes elastic deformation.

Figure 12: Comparison of empirical and simulated distortion. The 3 images on the left are actual prints that were obtained using our livescan system. The 2 images on the right were generated by applying the skin-distortion model to the normal impression in the middle.

Using the distortion model described above, along with our own enhancements that simulate changes in ridge thickness due to fingertip pressure, we have generated a database of simulated latent fingerprint images. The workflow diagram is shown in Figure 13. Creation of a new image begins with one or more real fingerprint images, typically slap or rolled prints. These prints are distorted automatically by our system, and the modified prints are used as the "foreground" of the new image. The system then selects a "background" image at random, adds noise to it, and then merges foreground with background to simulate the placement of a finger onto a physical surface. The result is a realistic latent fingerprint image that is added to the database.

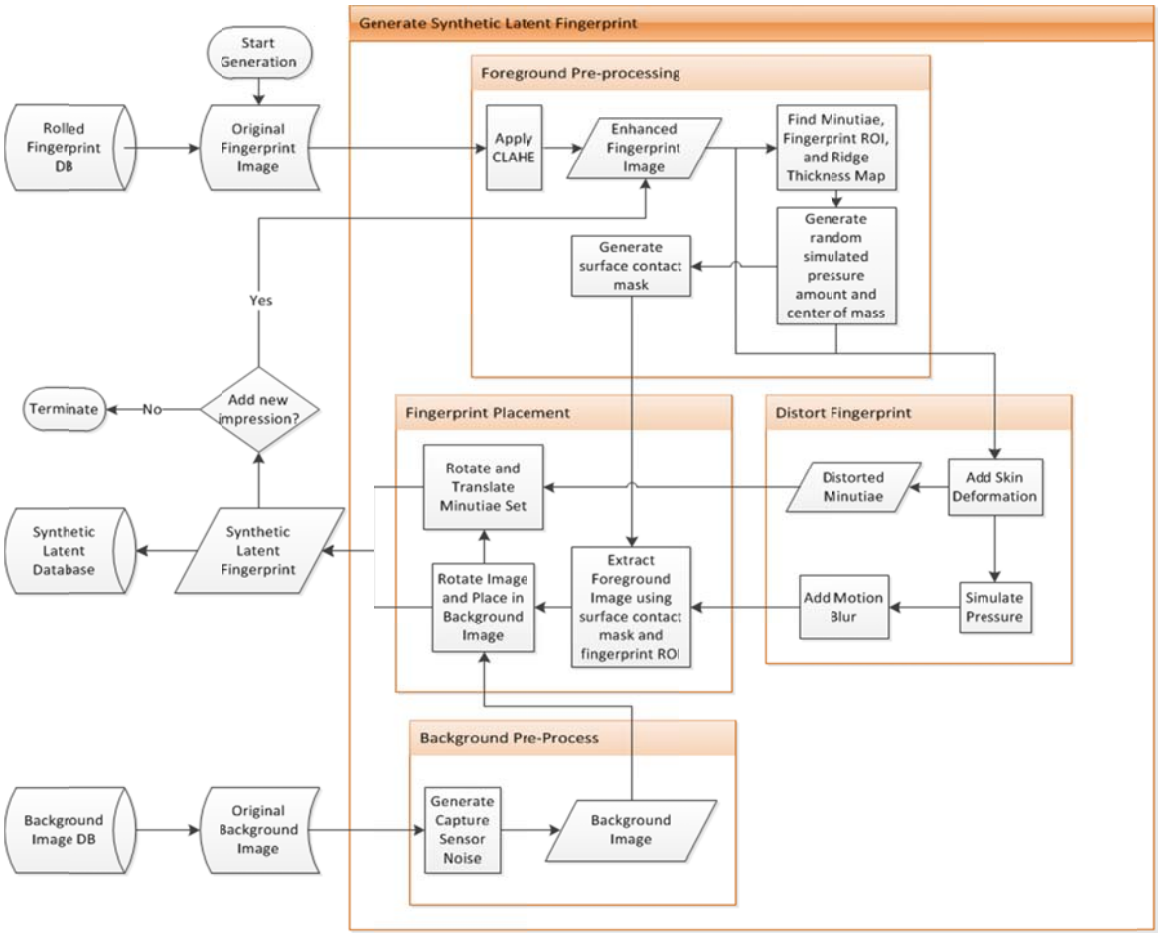

Figure 13: Workflow diagram for synthetic fingerprint image generation. Our system begins with images of rolled prints and a set of background images. For each new image to be added to the synthetic database, the system distorts one or more of the given fingerprint images, and separately applies distortion to a randomly selected background image. It then merges fingerprint(s) with the background to create a single composite image.

To support a fingerprint algorithm analysis workflow, we also proposed database schema and developed a digital library (DL) services model. With this model, researchers are able to investigate how an algorithm performs with synthetic, field-quality images. This framework was used to investigate the effect of image distortion parameters on feature extraction. The DL services model pairs new algorithms with image collections to allow analysis on which image characteristics affect algorithm performance. More details are provided in [43, 44].

II.4. Parallelization of feature analysis using GPUs

Section II.1 described our use of minutia triplets in the search for rare features. This section describes our high-speed implementation of minutia triplet matching using a General Purpose Graphics Processing Unit, often abbreviated as GPGPU or simply GPU. The process of matching against large databases using minutia triplets can take a significant amount of computational resources on a standard single-threaded Central Processing Unit (CPU). Fortunately, due to the nature of our hierarchical triplet-based approach,

the comparisons of fingerprints can be parallelized on a GPU, including 6-point and 9-point sets of minutiae.

Single-triangle (3-point) comparisons on the GPU. All triangles from a reference fingerprint, within certain size restrictions, are compared with all triangles of the remaining fingerprints in the database. For the reference image, each triangle side must be between 10 and 150 pixels in length. (These size restrictions do not apply to the images being compared.) Two triangles are declared to match if the following criteria are met:

- The perimeter of the test triangle is within 10% of the perimeter of the reference triangle;
- the smallest side length of the test triangle is within 10% of the smallest side of the reference triangle;
- both triangles have the same number of bifurcations, and therefore same number of ridge endings;
- the minutiae types on the largest sides of both triangles are the same;
- the minutiae types on the smallest sides of both triangles are the same;
- the sum of minuta angles (theta values) from both triangles agree to within 10%; and
- the smallest minutia angles from both triangles agree to within 10%.

On a standard CPU, matching is performed sequentially by comparing a single triangle from the reference fingerprint with all triangles from the remaining fingerprints, one at a time. In contrast, a GPU can launch multiple threads; in our implementation, each thread performs 32 such comparisons in parallel, and the result is stored as a 32-bit integer. A two-dimensional grid containing blocks of threads is launched, depending upon the number of triplet combinations of minutiae in the reference and in the fingerprint to be compared. In our implementation, each block consists of 256 threads.

In the first row of the grid, as illustrated in Figure 14, the first 256 triangles of the reference fingerprint are compared with all the triangles from the fingerprint being compared. In the second row, the next 256 triangles are compared. In the last row of the grid, the last 256 triangles of the reference fingerprint will be compared. For each blue box in the figure, the numbers represent triangles from the reference fingerprint, and the numbers in each orange box represent triangles from one of the fingerprints in the database. In each block, 256 triangles from the reference fingerprint are compared with 32 triangles from a compared fingerprint. In the figure, z represents the total number of triplet combinations in the fingerprint being compared.

Figure 15 illustrates the GPU block structure. The numbers in each blue box represent the triangle from a reference fingerprint, and the numbers in the orange box represent the triangles from the fingerprint being compared. In each thread, the reference triangle is compared with 32 triangles from the other fingerprint.

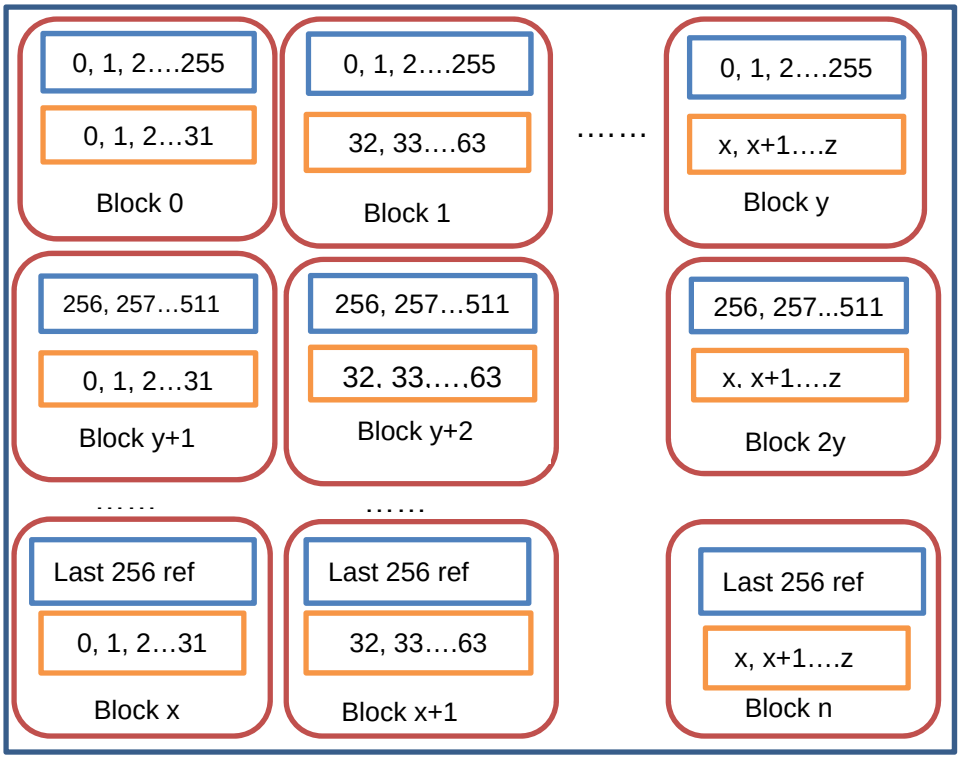

Figure 14: Grid layout on the GPU for 3-point matching.

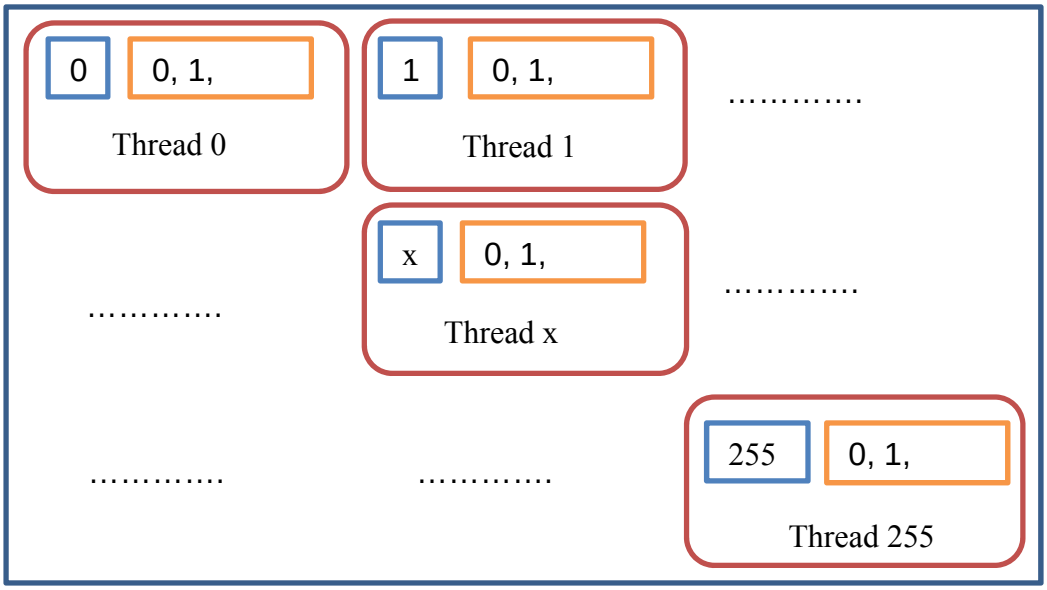

Figure 15: GPU block structure for 3-point matching.

Two-triangle (6-point) comparisons on the GPU. From the results of single-triangle comparisons, all of the triangles from the reference fingerprint that represent good matches with some triangles in the database fingerprints are used in 2-triangle sets. The reference triangle pairs are chosen so that no minutiae are shared. In addition to the single-triangle match criteria presented above, two triangles pairs are declared to match if the following criteria are met:

- No minutiae are shared between the two triangles;
- both triangle pairs have the same number of bifurcations, and therefore same number of ridge endings; and
- the distance between the centroids of the two triangles from the test image is within 10% of the centroid separation distance of the two triangles from the reference image.

For performing 2-triangle comparisons on the GPU, two arrays are formed such that the corresponding elements in both of the arrays are matched against triangles from the reference and compared fingerprint. Figure 16 illustrates the GPU block structure. Each box in the figure contains a pair of index values, with the first index representing a triangle from the reference image and the second index representing a triangle taken from a database image. In each block of the grid, each element from the reference and compared images is paired with all the other elements one by one and compared to find a match. All combinations of pairs of triangles are compared. The value n in the figure represents the total number of single-triangle matches. The number of pairs that can be formed in each thread is limited by $x = n/256$.

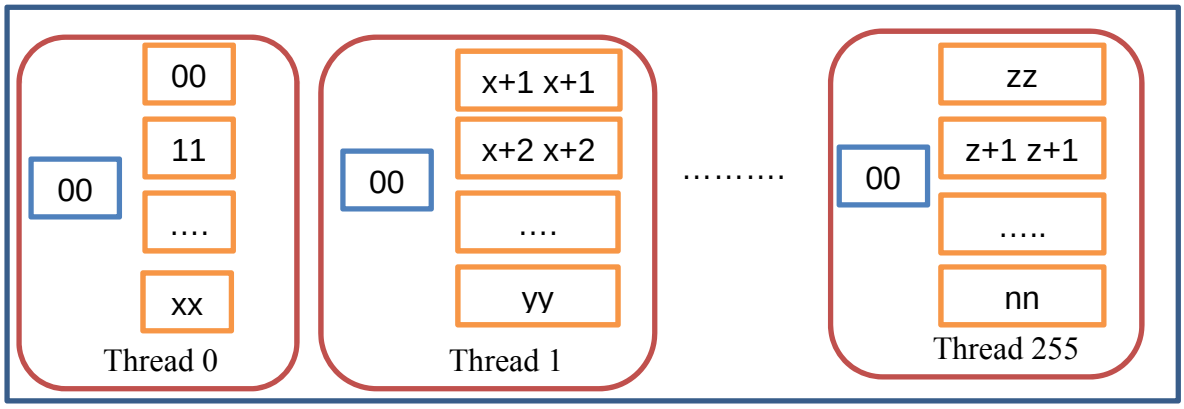

Figure 16: GPU block structure for 6-point (2-triangle) matching.

Three-triangle (9-point) comparisons on the GPU. Similar to two-triangle comparisons, triples of triangles are formed from the reference and test images. For reasons of efficiency, a triple is formed by adding a single triangle to a triangle pair that was found during 2-triangle matching. The reference three-triangle sets are chosen so that no minutiae are shared. In addition to the match criteria described above, two triangle triplets are declared to match if the following criteria are met:

- No minutiae are shared between the three triangles;
- both triangle triplets have the same number of bifurcations, and therefore same number of ridge endings; and
- the distances between the centroids of triangle pairs from the test image agree with those from the reference image within 10%.

In each block of the GPU kernel, all of the combinations with an element are formed and compared. Figure 17 provides a high-level illustration of the block structure for 3-triangle matching. Our GPU work is quite new, and has not yet been published. Experimental results are described briefly in Section III.4.

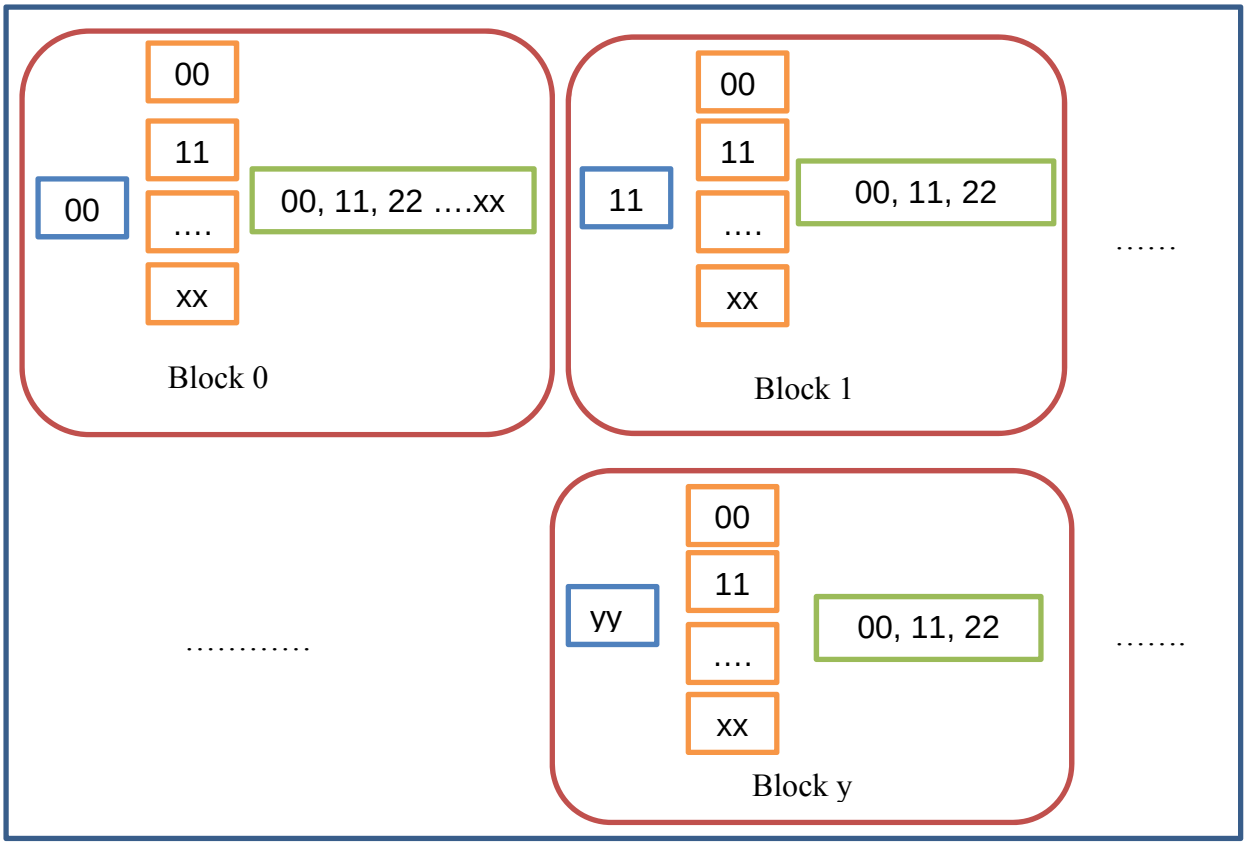

Figure 17: GPU block structure for 9-point (3-triangle) matching.

III. Results

This section presents results for the methods described in Section II.

III.1. Feature extraction and analysis

As described in Section II.1, we have developed new techniques for ridge extraction, minutia localization, minutia quality assessment, and use of extended feature sets based on minutia triplets.

Ridge extraction. Figure 18 presents results for our early work on ridge extraction [32]. The proposed algorithm was able to extract ridge connections as well as minutia directly from the grayscale image without any post-processing. In the figure, the left column shows example image windows. The middle column shows results of ridge extraction for those images, using a previously published ridge tracing method [13]. Notice that several ridge segments are not extracted correctly, because of problems associated with minutiae detection. The right column shows corresponding ridge segments that were detected with our new technique.

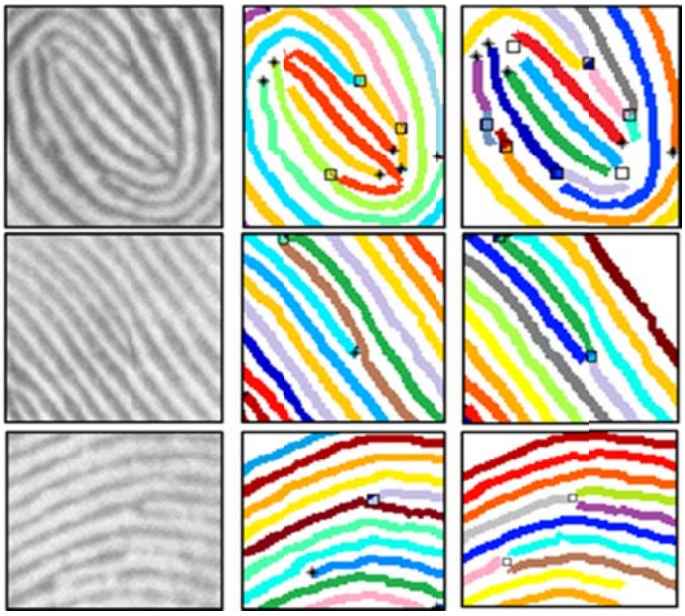

Figure 18: Results from ridge extraction with improved bifurcation determination. These images are from FVC 2000 DB1. From left to right, the columns represent example image windows, ridges extracted for those images using previously published methods, and ridges extracted with our new technique. The different colors indicate different ridge sections that were detected. Squares indicate bifurcations, while asterisks indicate ridge endings.

Minutia localization. Figure 19 presents examples of minutia localization using our new technique [39]. The proposed method was tested using the NBIS 3.2 MINDTCT minutia detection algorithm to find initial minutiae (although any detector could be used for this purpose). In order to demonstrate the importance of improved minutia localization, we performed image-to-image fingerprint matching using the original MINDTCT minutiae as well as minutiae that were refined using our new method. The NIST SD27 dataset was used, due to the available ground truth minutia sets. The database provides a set of 258 plain fingerprint images and 258 latent fingerprint images with minutiae determined manually by latent print examiners. All matching was performed using the NBIS Bozorth minutia-based algorithm [45].

Tables 1 and 2 show results of localization accuracy with the ground truth data provided by NIST SD27. The distance of each minutia from the NBIS and proposed methods to the corresponding ground truth minutia (determined by the closest minutia point) was calculated for all of the latent and plain prints in SD27. The "Mean distance to ground truth" is the average, over all minutiae in the fingerprint database, of the distance between the extracted minutiae and ground truth. The "% improvement" measures accuracy in minutia location, determined by the distance to the true minutia. Finally, the "% hit" measures the ratio of extracted minutiae which are exact matches with the ground truth to the total number of minutia in the ground truth set. In this test, any minutia point with a distance less than two pixels from the corresponding ground truth was labeled as an exact match.

Table 1 shows, on average, an improvement in accuracy of 4.67% for the plain print set and 6.44% for the latent print set when the proposed localization is performed. From the same table, we can see an improvement in exact matches from 8.92% to 15.5% for plain prints and 4.99% to 7.07% for latent prints when using the proposed method. From the plain database, 87.9% of the minutia sets improved in accuracy from the proposed localization method. The greatest individual improvement in accuracy of a minutia set (from a single fingerprint) was 14.1%. From the latent database, 88.4% of the minutia sets have shown an improvement in accuracy from the proposed localization method. The greatest individual improvement in accuracy of a minutia set (from a single fingerprint) was 24.3%.

Table 2 presents the same results for latent prints, but grouped by the pre-determined quality of fingerprint. These results show improvements in all categories when using the proposed method, with the largest improvement in the Ugly quality group. The improvement for the group of Ugly prints was 8.2% with an improvement for % hit from 4.65% to 7.9% after applying the proposed localization method. Since the quality designations were provided for the latent images only, the results for the plain print set are not considered here.

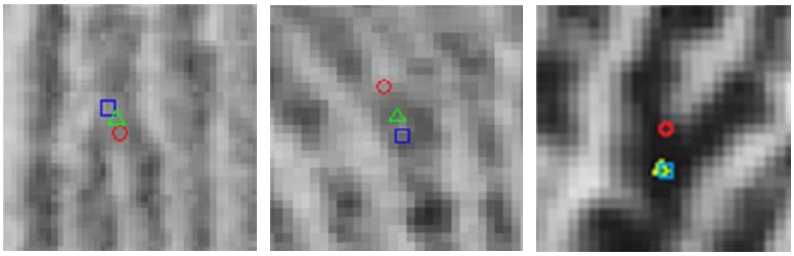

(a) (b) (c)

Figure 19: Examples of localized minutiae using the proposed method. These images are from NIST SD27. Blue squares are the manually extracted ground-truth points. Red circles are found from an AFIS feature extractor [45]. Green triangles are the improved, localized points from our approach.

Table 1: Localization accuracy results using NIST SD27 plain and latent prints with ground truth minutiae.

Print type	***Method***	***Mean distance to ground truth***	***% improvement***	***% hit***
Plain	NBIS	4.28	4.67	8.92
	Proposed	4.08		15.5
Latent	NBIS	4.66	6.44	4.99
	Proposed	4.36		7.07

Table 2: Localization accuracy results according to quality values assigned by NIST, using NIST SD27 latent prints with ground truth minutiae.

Print type	***Method***	***Mean distance to ground truth***	***% improvement***	***% hit***
Good	NBIS	4.48	4.70	6.81
	Proposed	4.27		9.44
Bad	NBIS	4.75	5.80	3.62
	Proposed	4.47		6.13
Ugly	NBIS	4.75	8.21	4.65
	Proposed	4.36		7.90

Quality assessment. This section presents results for quality assessment using FVC 2000 DB1 and NIST SD27. To demonstrate improved quality assessment, we created three groups based on the mean minutia quality: Good quality minutia sets ($50 \leq \overline{Q_m} \leq 100$), Bad ($25 \leq \overline{Q_m} < 50$), and Ugly ($\overline{Q_m} < 25$). The minutiae from NBIS MINDTCT are sorted using the quality score assigned, and then separately using the proposed quality score. An improvement in quality assessment would be indicated by higher matching scores in the good quality group and lower matching scores in the Ugly quality group.

Figure 20(a) shows an example output indicating the NBIS (red) and localized minutiae (blue). Part (b) of the figure shows a Receiver Operator Characteristic (ROC) curve indicating the False Accept Rate (FAR) vs. the True Accept Rate (TAR). Using the Equal Error Rate (EER) as a threshold, the graph indicates an increase in TAR from 69.3% to 74.6% and a decrease in FAR from 30.6% to 25.4% when using the proposed localization method. The net matching performance gain when using the localized minutiae is 10.5% for the good quality group.

Quality assessment results are shown in Figure 20 (c-d) and Table 3. The measurements from Table 3 come from the same test as Tables 1-2. Here, the quality measures of minutiae that were found to correspond with ground truth minutiae are shown for the NBIS quality measure and our proposed quality measure. The NBIS feature extractor finds many spurious minutiae, and we assume that higher quality measures should be found for those minutiae that have correspondences in the ground truth set. The results are shown for the three pre-determined quality groups and for the entire set. For the set of latent prints in SD27, the proposed method improved the average minutia quality for all 258 latent images by 14.62%. The group showing the most improvement was the Ugly group, with a 17.15% increase over the NBIS quality measure. From the plain fingerprint database, 98.8% of the prints have shown an improvement in quality assessment from the proposed method for minutiae that were successfully matched with the ground truth set, the largest individual improvement in quality assessment being 8.12%. From the latent database, 98.4% of the images have shown an improvement in quality assessment from the proposed method for minutiae that were successfully matched with the ground truth set, the largest individual improvement in quality assessment being 8.12%.

Figure 20(c) shows an example output indicating the NBIS (red) and localized minutiae (blue). In (d), an ROC curve is shown indicating improvement in quality assessment from the proposed method. In this experiment, the NBIS minutia set was used to generate matching scores for both test sets. However, the minutiae were automatically grouped based on the average minutia quality of the set using the NBIS quality measure and then again using the proposed method quality measure. The graph indicates an increase in matching performance of the Good quality group generated by the proposed method and a decrease for the Bad and Ugly groups. Using the EER as a threshold, the Good quality group TAR

increased from 95.9% to 97% and the FAR decreased from 4.1% to 3.0%, providing a net performance gain of 2.2% when grouping with the proposed quality assessment.

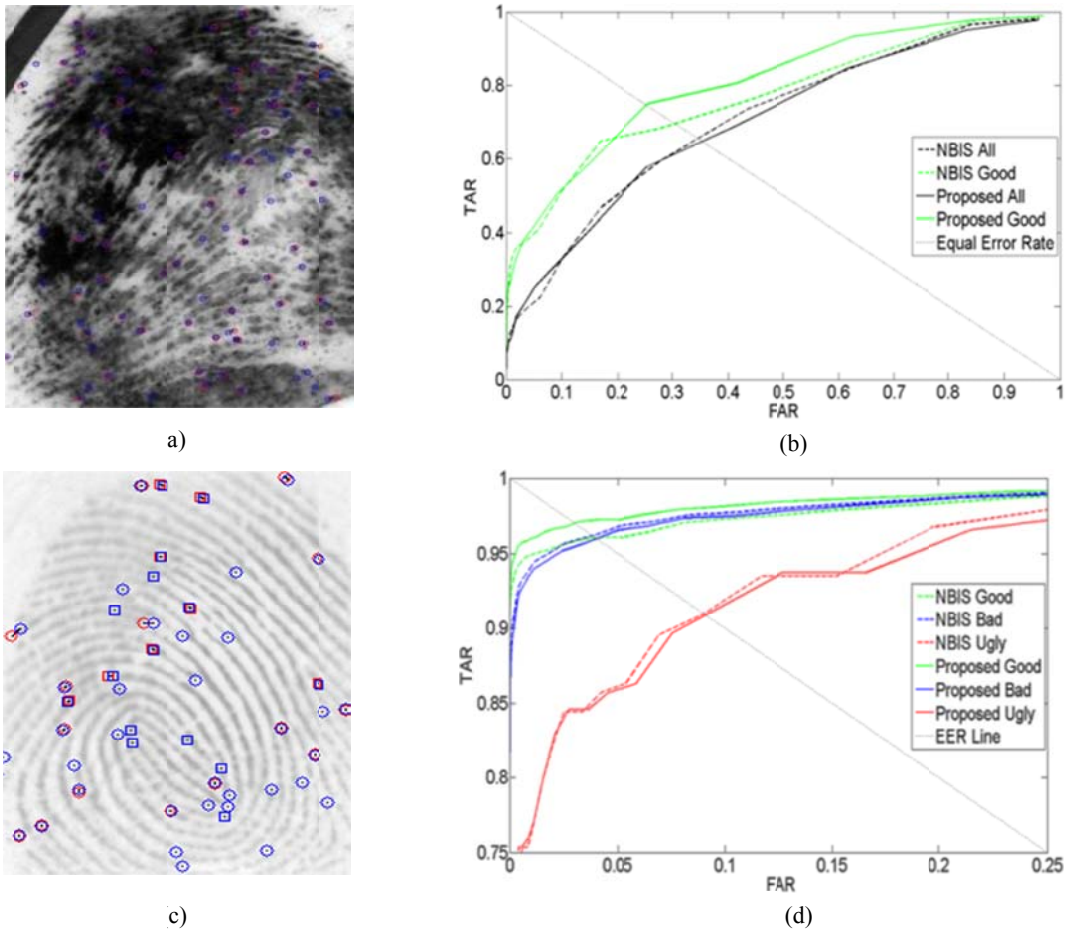

Figure 20: (a) Example image with localized minutiae from NIST SD27. (b) ROC curves describing the matching performance we obtained for NBIS and localized minutiae on NIST SD27 database. The diagonal line is the Equal Error Rate line. (c) Example image with localized minutiae from FVC 2000 DB1. (d) ROC curves indicating the match performance for quality groups using NBIS and our proposed quality assessment.

Table 3: Quality assessment accuracy using NIST SD27 latent prints with ground truth.

Print type	***Method***	***Quality***	***% improvement***
Good	NBIS	29.65	11.74
	Proposed	33.13	
Bad	NBIS	26.88	14.92
	Proposed	30.89	
Ugly	NBIS	30.50	17.15
	Proposed	35.73	
All	NBIS	29.01	14.62
	Proposed	33.25	

Extended feature sets. To visualize the distributions of the extended features described in II.1, a database provided by the FBI was used. The database contained 117,323 rolled and plain fingerprint images, of which the 83,815 rolled fingerprint images were used for analysis. A total of 9,675 images were removed for various reasons, such as low quality, too many spurious minutiae, or no friction ridge information available. This reduced the collection to 74,140 from which there were 2,575 different subjects providing multiple impressions of 23,942 unique fingerprints. The images were further partitioned into four groups, Very Good, Good, Bad, and Ugly as determined by the global image quality score assigned by Neurotechnology's VeriFinger software. This information is summarized in Table 4, where the quality level range is from 0 to 100. The minutiae distributions are shown in Figure 21 for each quality group. Only minutiae with a quality level greater than 40 were considered to be reliable.

Table 4: Summary of images contained in FBI Database

Group	**Quality Level**	**N**	$\bar{X}$	σ
Very Good	[75-100]	59,673	98.3	5.0
Good	[50-75)	6,836	63.2	7.2
Bad	[25-50)	5,042	38.4	7.2
Ugly	[0-25)	2,589	12.6	8.1

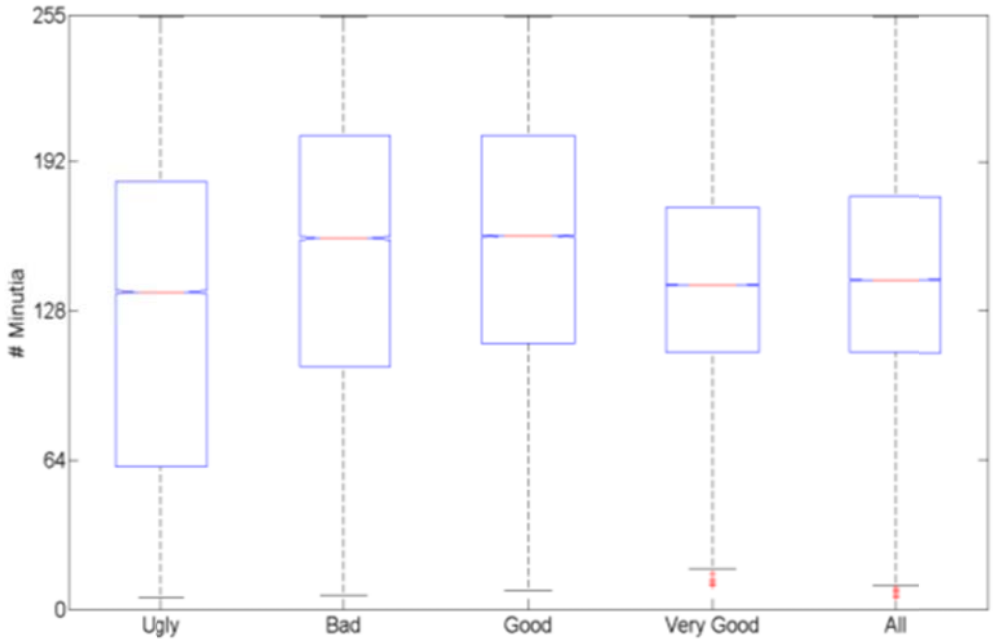

Figure 21: Box and whisker plot indicating minutia counts for the different fingerprint quality groups.

From the FBI database, we also found the ridge components associated with the minutia of each fingerprint. The distribution, indicating the probability in which a fingerprint in each of the respective groups has a certain number of ridge components, is shown in Figure 22. The figure reports complete ridge component counts in addition to any type of ridge component. In this case, a complete ridge component is one that originates and ends inside the fingerprint region of interest. An example of a non-complete ridge component is one that originates at a minutia and traces outside the fingerprint region of interest before a second minutia is reached. An example of this was shown in Figure 6, by the ridges connected to minutia H.

In addition, we also found the distribution of ridge cluster counts for each of the fingerprint quality groups, shown in Figure 23. These graphs indicate the expected number of ridge clusters that might be found within a given fingerprint image. As one might expect, the number of clusters increases as the quality increases, due to larger fingerprint surface area and more reliable features.

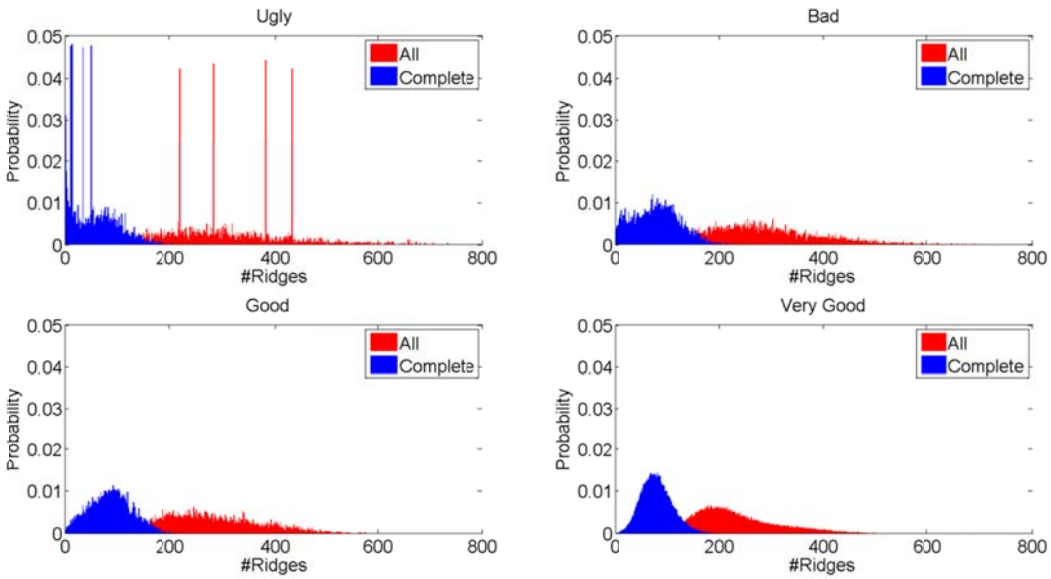

Figure 22: Ridge component counts for ridges wholly contained in the fingerprint region (Complete), and the entire set of ridge components (All) for each of the quality groups.

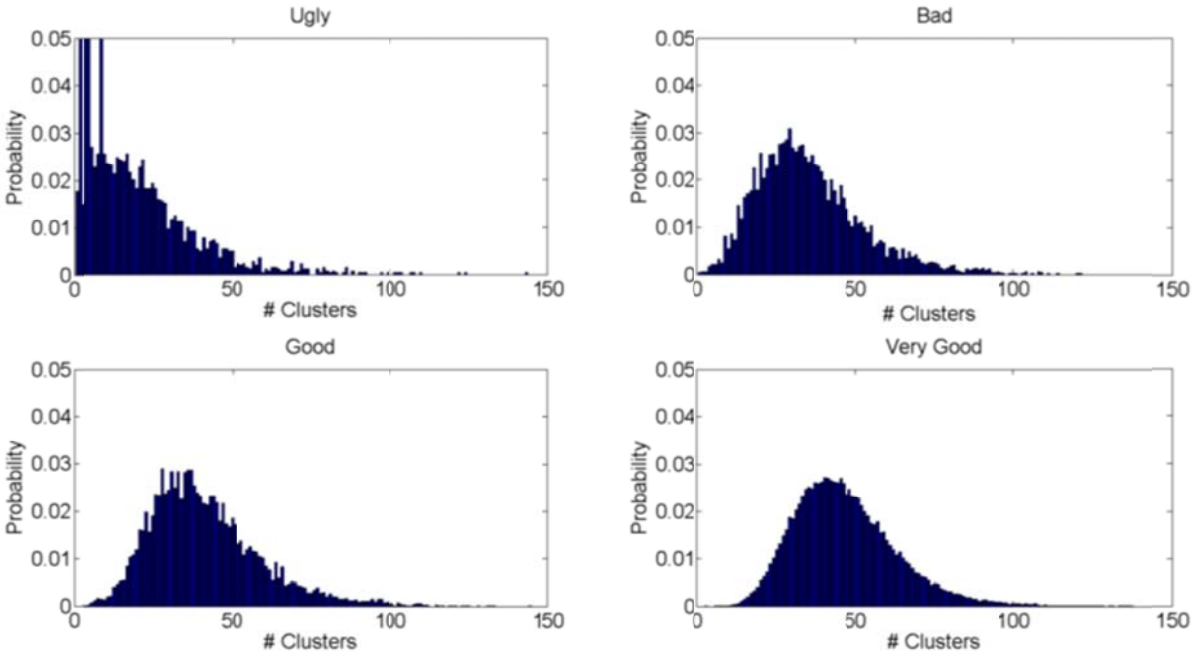

Figure 23: Ridge cluster count distribution for each of the quality groups.

Minutia triplets and rarity. Section II.1 described a method for mining distinctive features based on triples of minutiae, augmented with ridge information. We tested the approach in a preliminary study using 93 fingerprint images from the FVC2000 DB1 database, and more recently with 26,161 fingerprint images from the FBI database that was described earlier. The preliminary work is described more fully in [42], but the recent work with the FBI database has not yet been published.

In our first analysis, we mined for and discovered a set of 10 distinctive features within 93 images from FVC2000 DB1. Although the DB1 database provides multiple friction-ridge impressions from the same subject, we selected each image from a different subject. In the following discussion, we adopt this notation: "RC" refers to ridge count; "SR" refers to shared ridge segment; "sSR" refers to a short SR segment, with the requirement that the segment must be shorter than some distance *s*; "tRC" refers to total RC, or the sum of intra-RC + inter-RC for the feature; "SL" means side length; and "SSL" represents sum of side lengths. All distances are expressed in terms of pixels. (For this first set of experiments, the minutia direction was disregarded because the computed values were not reliable enough for our needs.) The distinctive features that we found are the following:

1) 2 triangles (6 minutiae), both triangles containing 2 sSR (each satisfying $s \leq 31$).
2) 2 triangles (6 minutiae), both triangles with intra-RC ≥ 35 and tRC ≥ 298.
3) 2 triangles (6 minutiae), both triangles large in size (SL ≥ 140 for each side), roughly equilateral (since the restriction exists that all side lengths are less than 150, and therefore the longest side length and the shortest side length could have a maximum difference of 10), and approximately equal RC on each side of the triangle (RC similarity parameter was set so that the RC had to be within 2 on all sides).
4) 3 triangles (9 minutiae), all triangles with intra-RC ≥ 35 and tRC ≥ 630.
5) 3 triangles (9 minutiae), all triangles large in size (SL ≥ 120 for each side), roughly equilateral (longest side length could only be 8 longer than the shortest), and approximately equal RC on each side of the triangle (RC similarity parameter was set so that the RC had to be within 2 on all sides).

6) 3 triangles (9 minutiae), all triangles having a small SSL to RC ratio (SSL/RC ≤ 17.37) with intra-RC ≥ 19.
7) 3 triangles (9 minutiae), all triangles having a small RC to SSL ratio (SSL/RC ≥ 65.04) with SSL ≥ 100.
8) 3 triangles (9 minutiae), each triangle containing a sSR (s≤ 60), and each triangle with intra-RC ≥ 39.
9) 3 triangles (9 minutiae), each triangle containing a SR, where there is a SR link between each triangle, and tRC ≥ 470.
10) 3 triangles (9 minutiae), each triangle containing a sSR (s ≤ 50), where there is a SR link between each triangle, and tRC ≥ 440.

Figure 24 shows an example of a distinctive feature (manually selected) that is similar to feature #10.

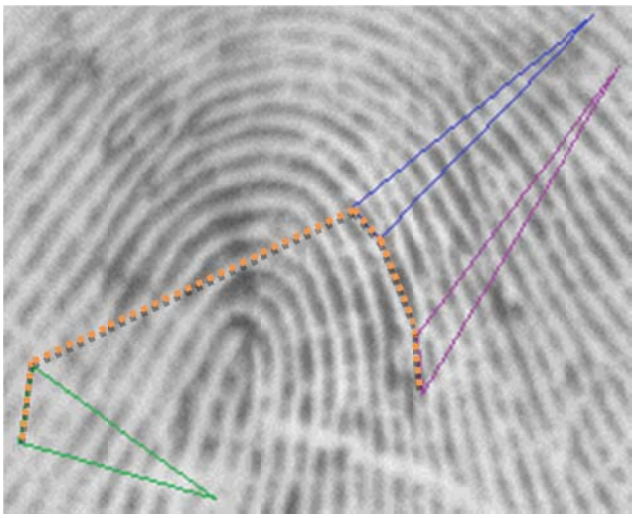

Figure 24: Illustration of distinctive feature from a 3-triangle set (manually selected). Short shared-ridge segments are present for each triangle, and the total ridge count is large. The shared ridge segments are between the minutiae connected by the dashed lines.

Based on the promising results from the first study, we began a second investigation that applied the same methodology to 26,161 images from the FBI database. To show the effect of tightening the constraints on matching, Figures 25-27 contain plots of the number of matches that result for single-triangle comparisons. One image from the database was chosen as the reference, and each of the remaining images was compared with it. The figures contain graphs for the first 1000 images only, so that the results are visible.

For Figure 25, all triangles from the reference image, within certain size restrictions, were compared with all triangles of the remaining fingerprints in the database. For the reference image, each triangle side was constrained to be between 10 and 150 pixels in length. (These size restrictions do not apply to the images being compared.) Two triangles were declared to match if the following criteria were met:

- the perimeter of the test triangle is within 10% of the perimeter of the reference triangle;
- the smallest side length of the test triangle is within 10% of the smallest side of the reference triangle;
- both triangles have the same number of bifurcations, and therefore same number of ridge endings;

- the sum of minutia-direction angles from the test triangle is within 10% of the sum of minutia-direction angles from the reference triangle;
- the smallest minutia-direction angle from the test triangle is within 10% of the smallest minutia-direction angle from the test triangle;
- the minutiae types on the largest sides of both triangles are the same; and
- the minutiae types on the smallest sides of both triangles are the same.

From Figure 25, it can be seen that the number of 3-point matches exceeds 100,000 for some images. The time taken for comparing each file was 120 ms, on average. The speed-up obtained by using GPUs when compared to sequential execution was 7.5.

For Figure 26, an additional constraint was placed on the matching process. In addition to the constraints listed above,

- each triangle is formed so that at least 2 minutiae belong to the same connected ridge component.

With this added restriction, the maximum number of matches has been reduced to 17,311. For Figure 27, additional constraints were incorporated into the matching process. In addition to the above,

- the sum of ridge counts between all triangle vertex pairs in the reference triangle must be the same as for the test triangle;
- the minutia types must match for the minutia pair in the reference triangle that has the fewest ridge crossings and the minutia pair in the test triangle that has the fewest ridge crossings; and
- the minutia types must match for the minutia pair in the reference triangle that has the most ridge crossings and the minutia pair in the test triangle that has the most ridge crossings.

The maximum number of matches has been reduced to 6,078, a dramatic reduction from the first case described above.

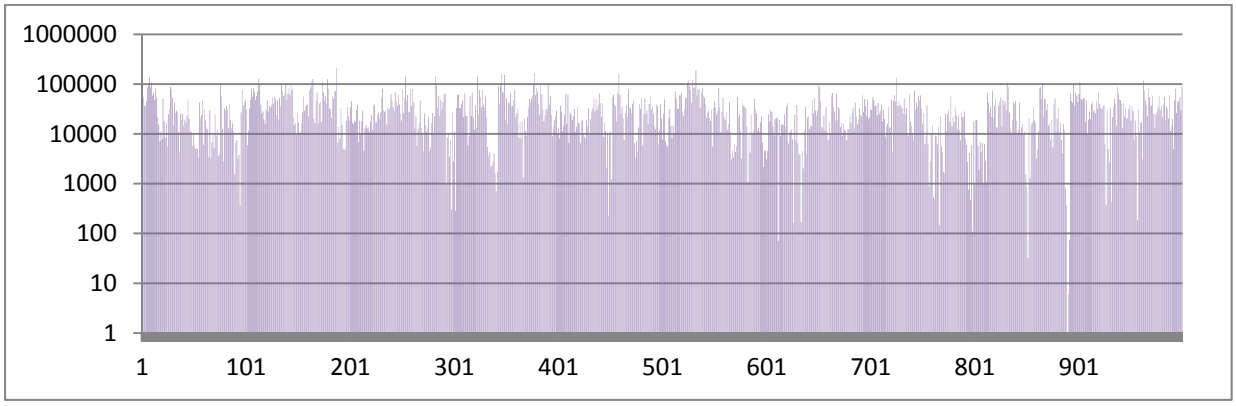

Figure 25: Number of single-triangle matches per image, for 1000 images. Comparisons were performed using a single reference image. The horizontal axis is the image index; the vertical axis indicates the number of triangles within each database image that have matches in the reference image.

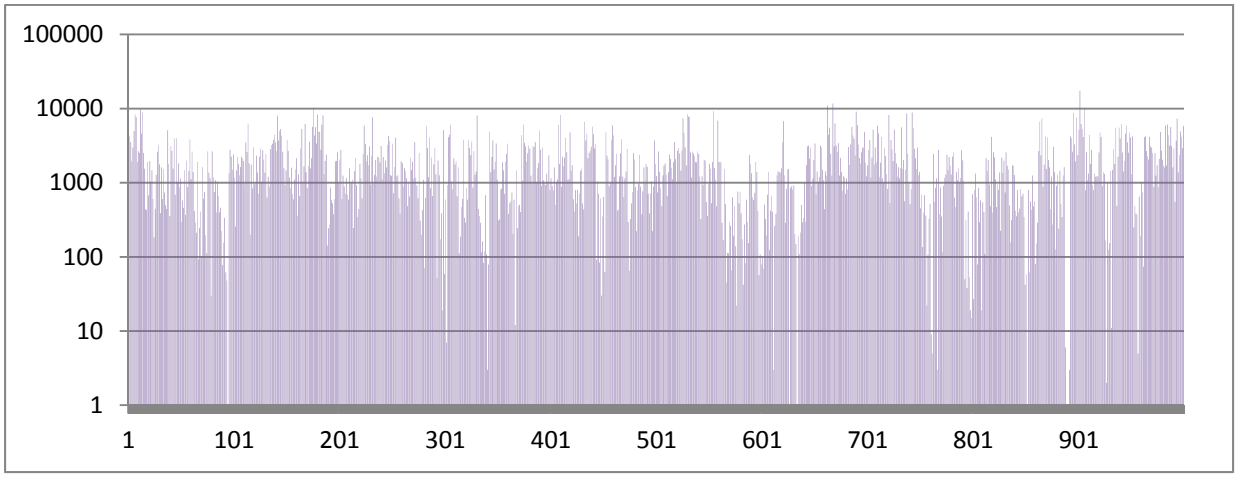

Figure 26: Same as the previous figure, except that each triangle is now constrained to contain 2 or more minutiae from a single connected ridge component.

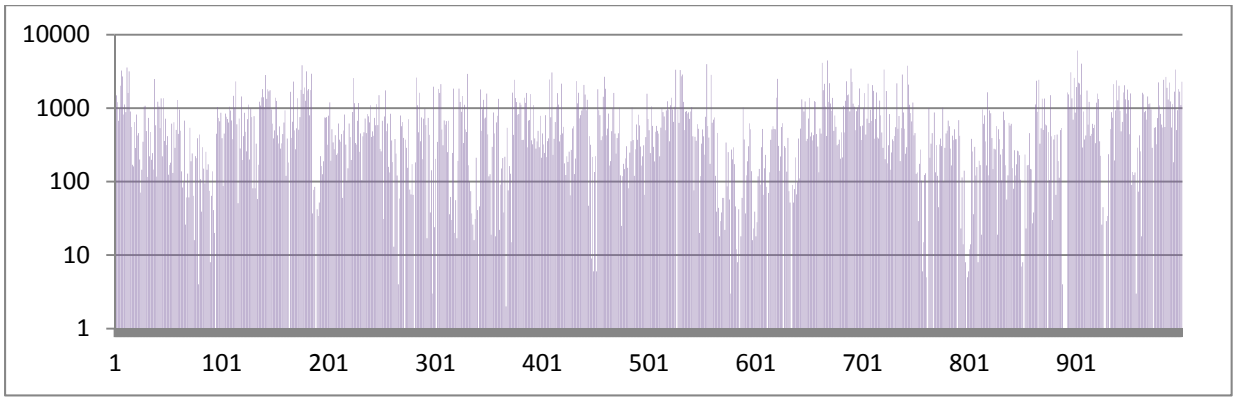

Figure 27: Same as the previous figure, except that ridge counts are considered during triangle matching.

Figures 28 and 29 illustrate the effect of extending the matching process from single triangles to 2-triangle sets and 3-triangle sets, respectively. Although the potential exists for more matches to be found, because the number of minutiae is larger, significantly more cases were found for which no matches to the reference image are present. By definition, such cases are rare, relative to this particular data set.

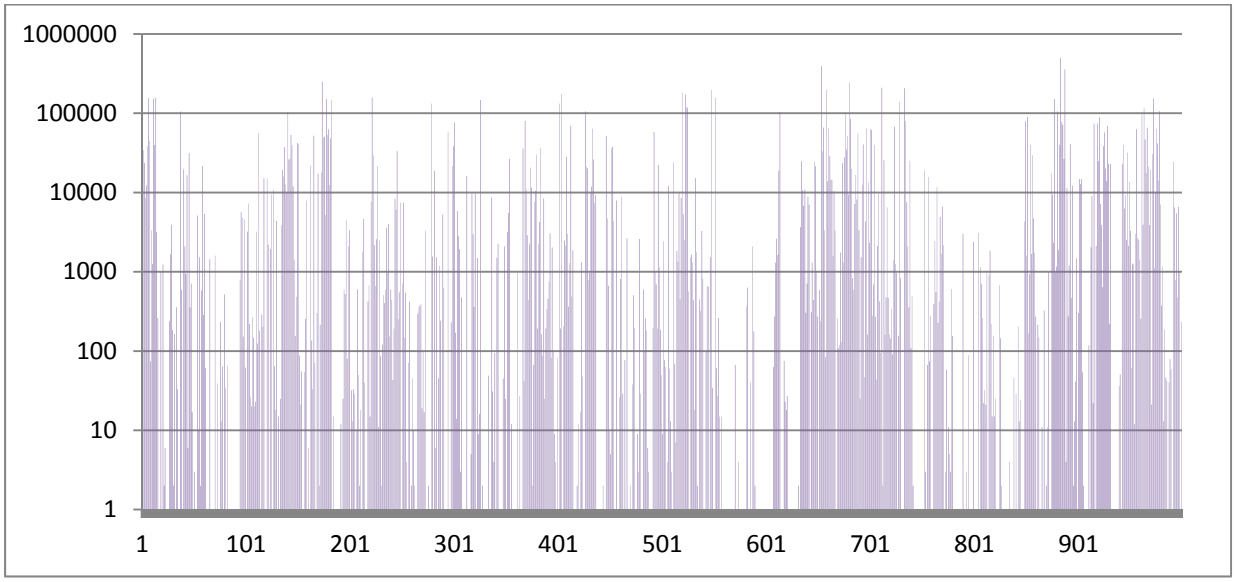

Figure 28: Number of two-triangle matches per image, for 1000 images. Comparisons were performed using a single reference image. The horizontal axis is the image index; the vertical axis indicates the number of cases within each database image that have matches in the reference image.

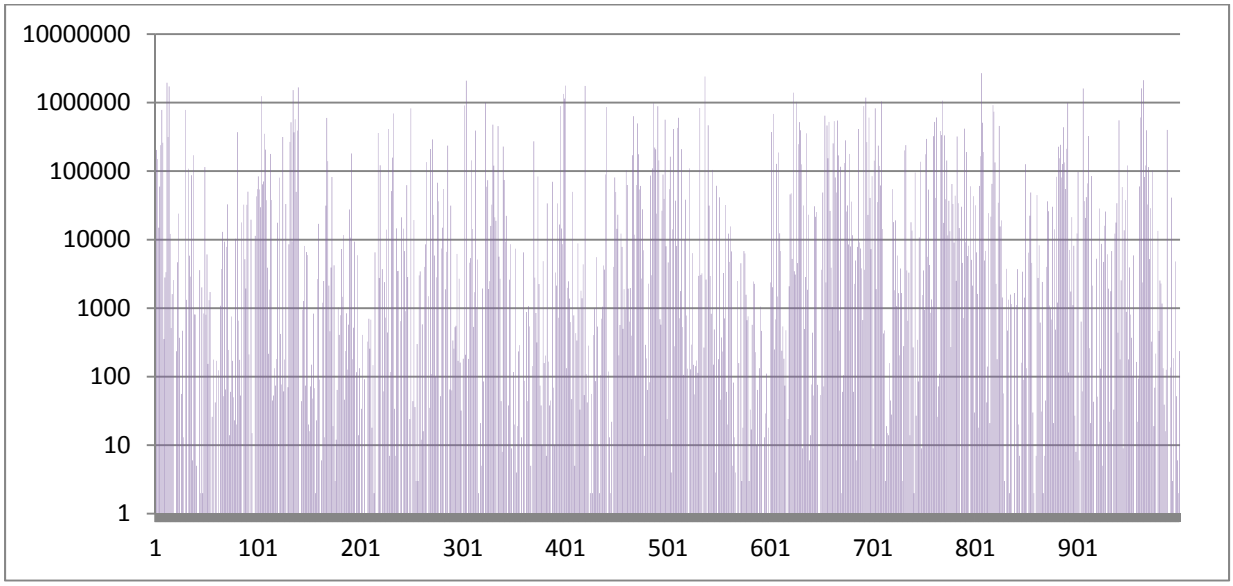

Figure 29: Number of three-triangle matches per image, for 1000 images. Comparisons were performed using a single reference image. The horizontal axis is the image index; the vertical axis indicates the number of cases within each database image that have matches in the reference image.

The previous figures presented statistics on an image-to-image basis. In another set of experiments, we selected triplet-based features from a reference image, and then searched for matches to those features within other images from the FBI database. Triangle side lengths were constrained to be between 10 and 150 pixels in length. The reference image contained 2,560 triangles, from which 3,275,520 six-point (2-triangle) features were formed. These were matched against 3,500 images of the database. (Time constraints did not permit an exhaustive search for this report, although work is in progress to complete the search using all remaining images from the database.)

Figure 30 shows the number of matches that were found for 1,048,576 of these six-point features. It can be seen that some of the 6-point combinations have very few matches. Although not indicated in the figure, several 6-point features from the reference image had no matches at all within these 3,500 images.

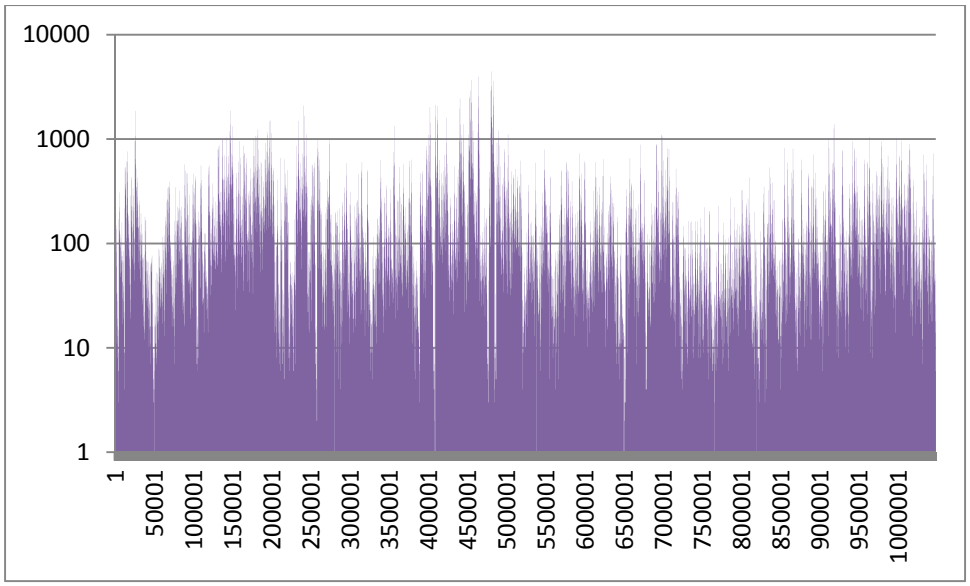

Figure 30: Number of matches per 6-point feature from a reference image. The horizontal axis is the index to a particular feature in the reference image; the vertical axis indicates the number of matches that were found in 3,500 images of the FBI database.

In summary, during this second investigation of distinctive-feature characterization we found several 6-point and 9-point features that are rare among 3,500 images of the FBI database. It was evident that some 6-point and 9-point features could be extremely rare, hence one needs not consider significantly higher numbers of minutiae to find rare features. As described in this section, ridge counts played an important role, and the features were constrained so that at least 2 minutiae from each triangle must come from the same connected component. Only high-quality minutiae were considered in this experiment, in order to reduce the likelihood of false rare features. Time constraints did not permit a more thorough characterization, such as matching against the full database, although that work will continue.

III.2. Quality assessment and segmentation of latent fingerprint images

The proposed segmentation algorithm, as described in Section II.2, was tested using a database of 258 latent fingerprint images [46]. For this database, ground-truth minutiae have been identified manually by

experienced latent examiners. The images also have been marked into three global quality scores, named Good, Bad, and Ugly as used earlier in this report. To test the proposed algorithm, we tabulated the number of true minutiae that were labeled by the segmentation routine as background. We also measured the detected fingerprint area that resulted from the proposed method, and compared it with the results from a typical segmentation algorithm. The ability to reduce the fingerprint area while also reducing the number of missed true minutiae shows the improved precision of the algorithm at fingerprint segmentation. When the fingerprint area is large and the number of missed minutiae is high, the segmentation has incorrectly labeled the background as foreground and vice versa.

In Figure 31(a-b), two latent fingerprint images from the database are shown. In (c-d), the detected fingerprint areas from the NBIS algorithm are shown [45], which uses a traditional method for segmentation. In (e-f), the segmentation from the proposed algorithm (without line removal) is shown. In (c-f), the background is indicated by the blacked out region. The dashed white outlines were drawn manually in (a-b), and are replicated in the other images to provide visual references for comparison. The figure demonstrates clearly that the detected fingerprint regions from the proposed segmentation algorithm are much smaller and more accurate than those of the previous method. From this figure, the ability of the proposed algorithm to reduce the searchable fingerprint area while improving accuracy can be seen.

The results shown in Table 5 are from a total of 5,303 true minutiae from the set of 258 latent images. The table shows the fingerprint area and percentage of true minutiae that were missed (determined to be in the background region) for the NBIS quality map and for the proposed quality map. The fingerprint area is a percentage of the entire image region. The goal was to reduce the fingerprint area while reducing or keeping the number of true minutiae labeled as background the same. P1 refers to the algorithm where thresholds were empirically set to have the same fingerprint area as the NBIS method. The results show the ability to reduce the percentage of true minutiae labeled as background from 1.41% to 0.29% when the fingerprint area is held constant. P2 shows the algorithm's ability to reduce the fingerprint area when the false negative rate is held constant. Here, the fingerprint area was reduced from 60.7% to 33.6% of the original image. Finally, P3 shows a scenario where both fingerprint area and missed true minutiae can be reduced by the proposed algorithm. These results show the ability of this approach to increase the accuracy of the segmented fingerprint area in latent images.

Figure 32 shows Receiver Operating Characteristic (ROC) curves for the proposed and traditional segmentation methods, using the same database of latent prints. The manually extracted minutiae provided with the data set were used for measuring match scores, and these results do not measure performance of automated minutia extraction methods. However, a minutia was removed if it was found to be in the background of the segmentation map for the respective method, indicating that regardless of the feature extraction method, the minutia would have been missed due to being labeled as background. The plot shows the True Accept Rate (TAR) vs. False Accept Rate (FAR) for both methods. The Equal Error Rate (EER) is shown for reference to indicate where the FAR equals the TAR. The closer the ROC curve is to the upper left of the graph, the better performance the method exhibits. Here, the traditional method produced a FAR of 33.8% and TAR of 66.2%. The proposed method produced a FAR of 32% and TAR of 68%. The net performance gain, when taking into account the gain in TAR and drop in FAR, was 3.6%.

Results from automatic line detection using the Hough-based approach can be seen in Figure 33 for two cases from SD27. In (a), two latent fingerprint images are shown on a structured background containing dark lines and text. The regions in the ridge flow map containing errors are indicated in (b), and (c) shows the detected lines from the image. Finally, (d) shows the corrected ridge flow direction in the region of interest. A size filter was applied to the detected lines, to remove those that were too small to be retained as line artifacts. The green lines indicate the final lines that were detected, and the red lines

indicate lines that were tentatively detected, but then rejected. The green lines were accepted for removal from the segmented fingerprint areas.

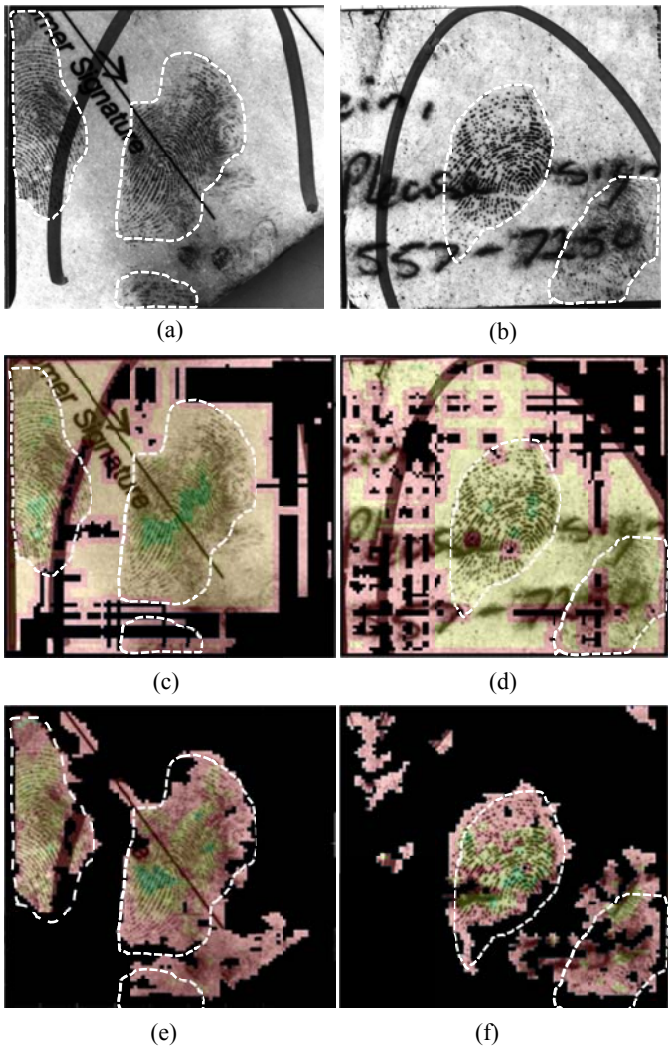

Figure 31: Examples of latent fingerprint segmentation. The dashed white boundaries were drawn manually to aid in comparison, and are the same in each column. Black regions represent background. (a-b) Original images from SD27 database. (c-d) Segmentation results from NBIS method. (e-f) Results from proposed method, which exhibit much better localization of friction ridges.

Table 5: Performance results for NBIS segmentation method and proposed method. The table indicates the detected fingerprint area as a percentage of the total image size. Also, the percentage of true minutiae labeled as background is reported.

	Fingerprint Area (% of total Image)	False Negatives (% of true minutiae labelled as background)
NBIS	60.7	1.41
P1	60.7	0.29
P2	33.6	1.47
P3	45.2	0.69

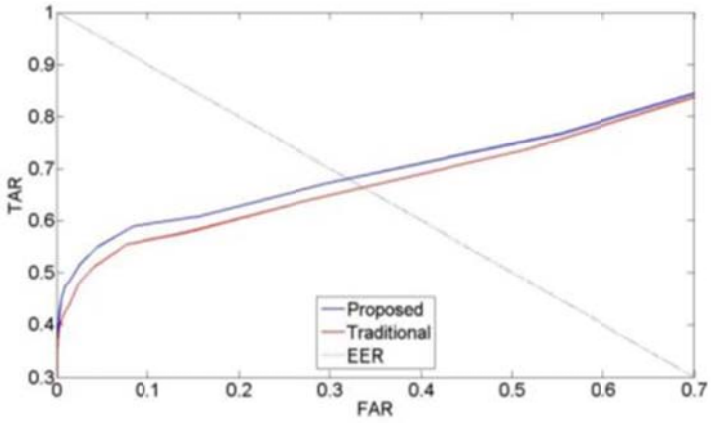

Figure 32: Graph showing ROC curve for proposed method and the traditional segmentation method. EER is indicated for reference and performance measurement.

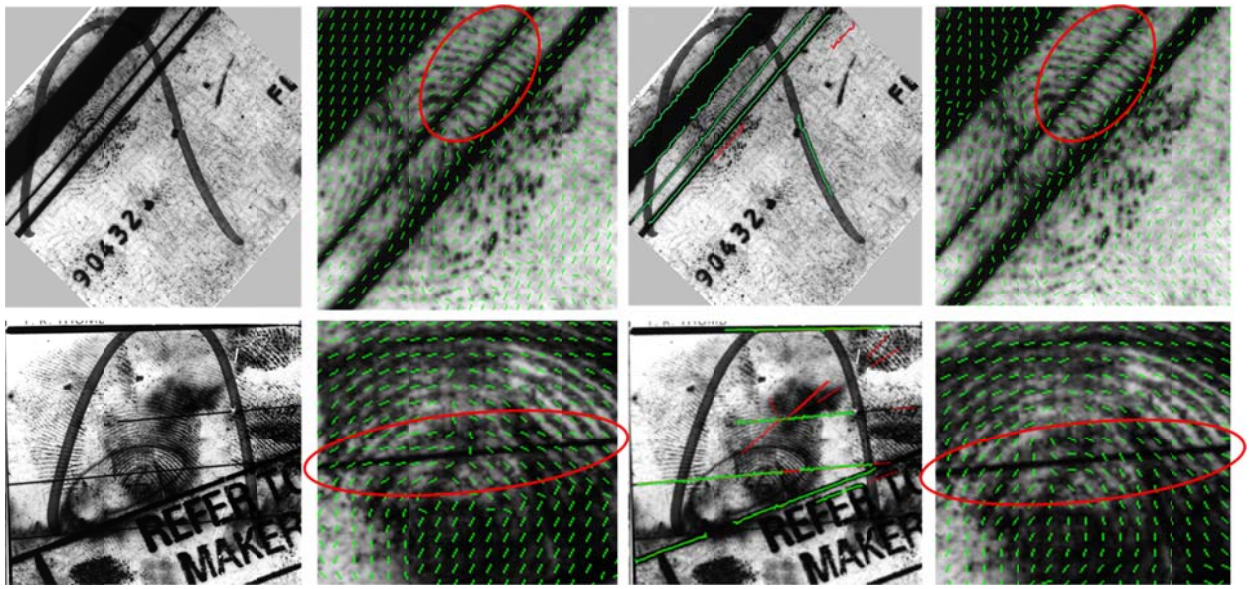

(a) (b) (c) (d)

Figure 33: Two examples of latent fingerprint images containing straight-line artifacts. (a) Latent print from SD27 database. (b) Error in ridge flow direction computation resulting from straight lines in background. (c) Detected lines using Hough-based method are shown in green, and red indicates lines that were considered but rejected as artifacts. (d) Corrected ridge flow direction in the marked region around the detected line.

III.3. Distortion modeling and creation of a synthetic image database

We have generated a synthetic latent fingerprint database following the procedures outlined in Section II.3. To avoid issues related to privacy, we used the public domain fingerprint image database, NIST Special Database 27, as our source for initial fingerprint images. From the 258 good-quality rolled prints in SD27, our system automatically generated a database of 2,360 images containing a total of 4,725 latent fingerprint impressions. This database will be made available to researchers, practitioners, and others who are interested in latent print analysis.

The full size of the database is 7.8 gigabytes. This large size results from the realistic sizes of the impressions and backgrounds, which were chosen to match the standard resolution of fingerprint images, 500 dpi. Images in the database represent a surface area ranging from approximately 1 inch × 1 inch up to 3.5 inches × 5 inches. The image files are stored using the common TIFF standard with lossless compression.

A few example images from this database are shown in Figure 34. Creation of a new image for our database began with a real fingerprint image taken from SD27. That image was distorted by our system as described in II.3, to become part of the "foreground" of the new image. Our software selected a "background" image from a collection of copyright-free images, and applied distortion separately to the background. The foreground was then merged with the background to create a realistic latent fingerprint image.

Parameters required by the distortion methods were selected empirically, with the goal of ensuring that the resulting synthetic database would have statistics that are close to those of the latent prints in the SD27 database. Figure 35 contains box-and-whisker plots that show very similar distributions of minutia counts in both latent databases.

(a) (b) (c)

Figure 34: Examples of synthetically generated latent fingerprints of varying quality. (a) Rolled exemplars from NIST SD27 were used as the input images. These were distorted and then merged with background images to create (b) new, realistic latent fingerprint images. (c) Ground-truth minutiae are provided with the database, and are shown here superimposed over close-up views of the database images.

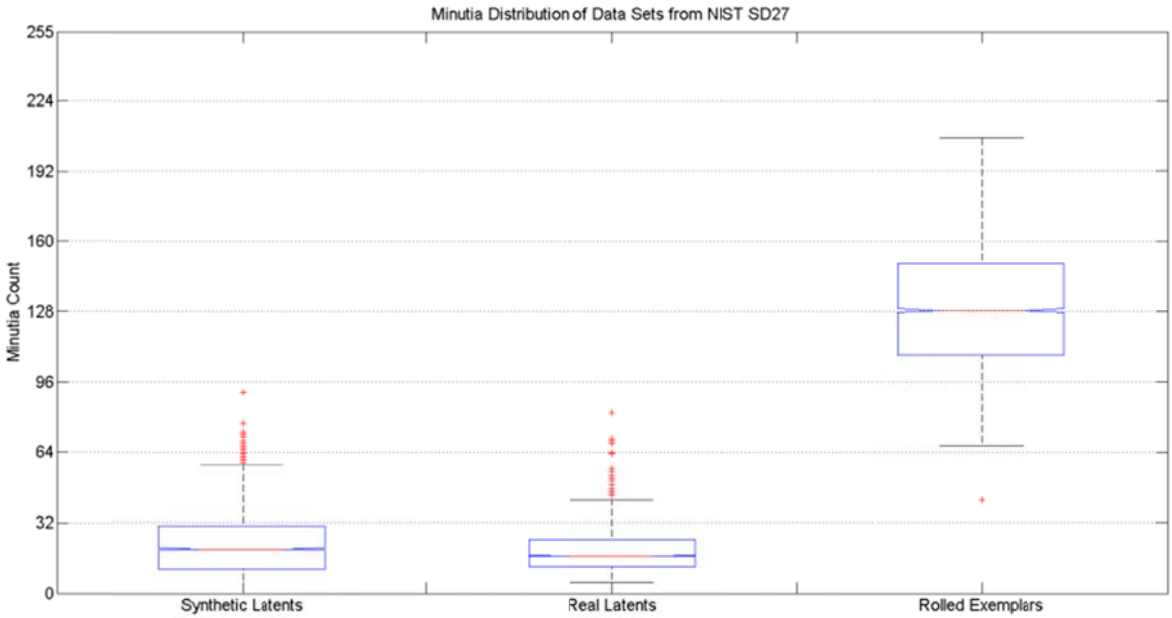

Figure 35: Comparison of minutia counts in (left) our synthetic database of latent prints, (center) actual latent prints in NIST SD27, and (right) rolled prints in SD27. These rolled prints were used by our system to generate new latent prints for our database. The distributions of minutia counts are very similar for both latent databases.

III.4. Parallelization of feature analysis using GPUs

We conducted experiments to observe the improvement in computation time for our algorithm with a Graphics Processing Unit, as introduced in Section II.4. This section describes the improvement in processing speed that was achieved. (The results of matching were described separately in Section II.1.)

Table 6 presents results related to computation time for matching of single triangles (3 points) and two triangles (6 points), in separate runs using a standard single-thread machine (CPU) and a GPU. In each case, minutiae from a reference file were compared with those from 24 other fingerprints. These other prints are labeled file 2 through file 25 in the table. Minutiae were not shared between triangles; the type of minutia was considered in the comparison (ridge ending vs. bifurcation); and triangle-to-triangle centroid distances were considered.

As an example, consider the results for file 25. This fingerprint contained 47 minutia points, from which 16215 different triangles were formed. On the CPU, single-triangle matching between this file and the reference file took 360 ms, while 6-point (two-triangle) matches required 9190 ms. When we ran the matching algorithms for this pair of fingerprint images on the GPU, the run times for single- and two-triangle matching were reduced to 50 and 1480 ms respectively. The GPU was therefore 7.2 times faster for this image pair for single-triangle matching, and 6.2 times faster for two-triangle matching.

The last row of the table shows the average improvement for both cases, and for all 24 comparisons. On average, the speedup obtained for single-triangle comparisons was 7.6, and for two-triangle comparisons the speedup was 6.5.

Table 6: Results of parallelizing single-triangle and two-triangle comparisons on a GPU. Each row represents a single fingerprint file. The first columns contain a file identifier, number of minutiae in that file, and number of minutia triples. The columns for T_s list the amount of time required to perform single-triangle matches, T_p is the time for two-triangle matches, $Speedup_s$ is the improvement for single-triangle matches, and $Speedup_p$ is the improvement for two-triangle matches. T_s, and T_p are in milliseconds.

			CPU		**GPU**					
File	*No. min.*	*No. of triplets (triangles)*	T_s *(ms)*	T_p *(ms)*	T_s *(ms)*	T_p *(ms)*	*Grid size single*	*Grid size pairs*	*Speed -up$_s$*	*Speed-up$_p$*
Ref. file	33	5456								
File 2	38	8436	190	4770	60	760	22x64	129x129	3.1	6.2
File 3	29	3654	80	350	20	50	22x115	67x66	4.0	7.0
File 4	17	680	10	70	10	10	22x22	45x45	1.0	7.0
File 5	41	10660	260	4580	30	710	22x334	128x128	8.7	6.5
File 6	33	5456	140	2550	20	360	22x171	111x111	7.0	7.1
File 7	51	20825	550	33310	60	5570	22x651	209x209	9.1	6.0
File 8	44	13244	280	22210	30	3830	22x414	192x192	9.3	5.7
File 9	23	1771	50	270	10	40	22x56	63x63	5.0	6.8
File 10	23	1771	50	140	10	20	22x56	52x51	5.0	7.0
File 11	32	4960	120	350	10	50	22x156	66x66	12.0	7.0
File 12	25	2300	60	580	10	80	22x72	76x76	6.0	7.3
File 13	22	1540	40	150	10	20	22x49	54x53	4.0	7.5
File 14	28	3276	90	650	10	90	22x103	78x78	9.0	7.2
File 15	34	5984	160	2870	20	450	22x188	116x115	8.0	6.5
File 16	42	11480	320	13740	30	2390	22x359	171x170	10.7	5.7
File 17	43	12341	310	9580	30	1550	22x386	154x153	10.3	6.1
File 18	50	19600	440	7880	60	1250	22x613	146x145	7.3	6.3
File 19	42	11480	310	3230	30	500	22x359	117x117	10.3	6.5
File 20	34	5984	140	1750	10	230	22x188	101x101	14.0	7.6
File 21	39	9139	240	3540	20	530	22x286	119x119	12.0	6.6
File 22	22	1540	40	70	10	10	22x49	43x42	4.0	7.0
File 23	49	18424	410	36330	40	6740	22x576	216x215	10.3	5.4
File 24	53	23426	570	40630	60	7750	22x733	221x221	9.5	5.2
File 25	47	16215	360	9190	50	1480	22x507	151x151	7.2	6.2
Average Speedup									7.6	6.5

III.5. Summary

We have addressed the problem of sufficiency through several related research thrusts. In the area of *feature extraction* we developed new methods of grayscale image analysis for detecting ridges and for improving the localization (and therefore the quality) of ridge endings and bifurcations. From the point of view of sufficiency for latent prints, grayscale analysis is important because inherently more information is available than with traditional approaches that are limited to binary analysis. We have validated our contribution using public-domain as well as commercial software products that perform feature detection and matching.

Another research thrust related to feature extraction has been the evaluation of features, particularly "extended" features based on minutia triplets, for their suitability in identification/exclusion tasks. We developed a methodology for evaluating triplet-based distributions of minutiae together with ridge connectivity and ridge crossings. (These minutiae and ridges were detected using the techniques described in the previous paragraph.) We followed the principle that features carry more discriminating power if they are statistically rare. We tested the methodology first with a small set of 100 fingerprint images, and later with a much larger image database. Time limitations did not permit an exhaustive evaluation with the larger database, but did lead to features based on 6-point minutia sets using 3500 fingerprint images.

Another research thrust directly addressed the problem of quality-based *image segmentation* of latent prints. Building on our investigation of grayscale image analysis, we developed an approach for assigning quality scores to detected ridges, and from those scores to estimate the extent of the foreground region of the image. An unusual aspect of our approach has been to incorporate a line-detection algorithm directly into the segmentation process. This was motivated by examples in the SD27 database, for which many of the image backgrounds contain straight-line artifacts. Many existing systems are "fooled" by these lines because they closely resemble friction ridges. We demonstrated that our system can detect many of these lines in advance, and can use that information to improve the accuracy of the computed ridge flow, which in turn leads to improved image segmentation.

Distortion modeling represents another thrust of our research. We investigated fingerprint image distortion in part because of our stated project goal of synthesizing a database of realistic latent images. The resulting database contains more than 2000 images with more than 4700 fingerprint impressions on realistic backgrounds. This database will be made available to researchers and practitioners who are interested in latent print analysis.

Finally, *high-speed implementation* has been another research thrust. Our GPU-based implementation has been instrumental in characterizing the triplet-based features described above. The motivation for this aspect of the work has not been to improve existing techniques, but instead to assist in completing our investigation in a timely fashion.

IV. Conclusions

IV.1. Discussion of findings

The results obtained through our research have been noteworthy. First, we have developed a novel hierarchical, triplet-based representation among minutiae and associated friction ridges. Such a representation offers a unique and powerful way for fingerprint search and comparison. In addition, it allows for the mining and detection of unique and rare features that can be extremely useful when estimating the statistical likelihood of a match with a given print. For instance, we have identified statistically rare features among various prints in a database. Likewise, given a feature, our method also allows for assessing if the feature would be considered rare. We have begun to parallelize the algorithms on low-cost general purpose graphics processing units (GPUs), and significant speedups have been achieved. By parallelizing the algorithms, we believe much larger databases can be handled. We also have been successful in developing techniques to enhance the accuracy of extraction of ridges and minutia from a print, using novel filtering techniques. Finally, we have successfully created databases of synthetic fingerprints. These achievements are all aligned with our goals and objectives.

IV.2. Implications for policy and practice

The interpretation of friction ridge pattern evidence is based primarily on experience, and a large component of the process is subjective. In addition, training is accomplished in-house and varies substantially from laboratory to laboratory. There is no nationwide standardized education and training curriculum. The differences in training and experience can result in quite varied interpretations of the same evidence by different practitioners, and such differences may impact inculpation and exculpation of suspects and more importantly impinge on the tenet of the presumption of innocence. Confounding the interpretation is a lack of documentation regarding validation of the processes. Validation is essential for determining the limitations of a process or methodology so that practitioners have data to establish guidelines to not exceed the bounds of the system when subjectively interpreting evidence. The interpretation process also is problematic because the quality of the evidence varies substantially, ranging from highly informative and resolved to partial, smudged, and distorted. Lastly, the quality and quantity criteria for a "print" to meet a sufficiency threshold for interpretation and subsequently for an identification are not defined. Although acceptance of latent print evidence has been accepted in the Courts, legal admissibility is a poor criterion for scientific quality. We all must accept that there are inherent limitations with the current process that need to be improved. These gaps in the system must be addressed.

The studies herein address some aspects of image quality problems related to identifiable Level 1, 2, or 3 details and how such data can be utilized to support the subjective interpretations that to date may not have been validated sufficiently. Moreover, the uncertainty and possibility of error that potentially may contribute to some practitioners actions to "push the envelope" may soon be able to be quantified so fact finders and triers of fact can be better informed on the vagaries, so justice may be better served.

From a policy perspective, the work reported herein lays a foundation for further development so that sufficiency metric(s) can be developed. However, far more effort is required for development of a more objective based support system for interpretation of friction ridge detail. Although not yet complete, the data herein should be considered as part of a more comprehensive training program to promote understanding, increasing accuracy and reliability, and more uniform assessment of fingerprint pattern analysis and practice.

IV.3. Implications for further research

The early research performed here lays a robust foundation for the transition to late-stage research and then development, on a path to testing and validation and transition to a useable "tool kit" by

practitioners. If this were to occur, the first step in this process could be to apply the emerging techniques to the large data set of digitized fingerprint images of varying quality that we acquired from the FBI (118,000 anonymized images from 2600 individuals, classified as to quality by the FBI as "Good, Bad and Ugly"), and characterize and measure the performance of our methods and modify or improve them. The results from this effort would be published. The next step would be convert our concepts into prototype methods and involve forensic fingerprint examiners with varying degrees of expertise and experience in rigorously structured experimentation with the methods following training on them. This effort would allow us to determine whether or not these techniques could be transitioned to use. This, too, would be published. From these two efforts, an initial protocol could be constructed and subjected to extensive and rigorous forensic validation, including by others.

Our novel research approach deserves also consideration for extension to other pattern evidence analysis problem sets, most of which require a determination of sufficiency as a crucial step. In fact, though the formal step to determine sufficiency through the ACE-V process is most often used in conjunction with fingerprint analysis, it applies to the human forensic comparative examination of pattern evidence such as shoeprint, tire tread, documents, and projectiles (e.g., bullets). Throughout the history of these forensic pattern disciplines, a subjective determination of sufficiency has occurred and persists to this day. If our approach was extended through additional research pursuits, a universal approach to providing a quantitative basis for determining and communicating sufficiency might be achievable.

IV.4. Acknowledgement

The PIs gratefully acknowledge the Criminal Justice Information Services Division (CJIS) of the Federal Bureau of Investigation for providing a database of 117,323 rolled and plain fingerprint images. These images have been very helpful in validating the results presented in this report.

V. References

[1] D. R. Ashbaugh, *Qualitative-Quantitative Friction Ridge Analysis: An Introduction to Basic and Advanced Ridgeology*. Boca Raton, FL: CRC Press, 1999.

[2] M. R. Hawthorne, *Fingerprints: Analysis and Understanding*. Boca Raton, FL: CRC Press, 2009.

[3] Scientific Working Group on Friction Ridge Analysis Study and Technology (SWGFAST). (2002). *Friction Ridge Examination Methodology for Latent Print Examiners*. Available: www.swgfast.org.

[4] Scientific Working Group on Friction Ridge Analysis Study and Technology (SWGFAST). (2004). *Standards for Conclusions*. Available: www.swgfast.org.

[5] J. R. Vanderkolk, "Forensic Individualization of Images Using Quantity and Quality of Information," *Journal of Forensic Identification,* vol. 49, pp. 246-251, 1999.

[6] D. R. Ashbaugh, "The Premises of Friction Ridge Identification, Clarity, and the Identification Process," *Journal of Forensic Identification,* vol. 44, pp. 499-516, 1994.

[7] L. Haber and R. N. Haber, "Scientific Validation of Fingerprint Evidence under Daubert," *Law, Probability and Risk,* vol. 7, pp. 87-109, 2008.

[8] J. Thornton, "Setting Standards in the Comparison and Identification," *Proc. 84th Annual Training Conference of the California State Division of the International Association of Identification*, Laughlin, Nevada, May 2000.

[9] D. L. Grieve, "The Identification Process: SWGFAST and the Search for Science," *Journal of Forensic Identification,* vol. 50, pp. 145-161, 2000.

[10] E. Tabassi, C. Wilson, and C. Watson, "Fingerprint image quality," NIST Internal Report 7151, August 2004.

[11] S. Lee, H. Choi, K. Choi, and J. Kim, "Fingerprint-Quality Index Using Gradient Components," *IEEE Trans. on Information Forensics and Security,* vol. 3, pp. 792-800, 2008.

[12] J. Fierrez-Aguilar, Y. Chen, J. Ortega-Garcia, and A. K. Jain, "Incorporating Image Quality in Multi-algorithm Fingerprint Verification," *Proc. International Conference on Biometrics (ICB 2006)*, Hong Kong, China, 2006, pp. 213-220.

[13] D. Maio and D. Maltoni, "Direct Gray-Scale Minutiae Detection in Fingerprints," *IEEE Trans. on Pattern Analysis and Machine Intelligence,* vol. 19, pp. 27-40, 1997.

[14] X. Jiang, W.-Y. Yau, and W. Ser, "Detecting the Fingerprint Minutiae by Adaptive Tracing the Gray-level Ridge," *Pattern Recognition,* vol. 34, pp. 999-1013, 2001.

[15] J. Liu, Z. Huang, and K. L. Chan, "Direct Minutiae Extraction from Gray-Level Fingerprint Image by Relationship Examination," *Proc. 7th International Conference on Image Processing*, pp. 427-430, 2000.

[16] J. Feng, Z. Ouyang, and A. Cai, "Fingerprint Matching using Ridges," *Pattern Recognition,* vol. 39, pp. 2131-2140, 2006.

[17] A. N. Marana and A. K. Jain, "Ridge-Based Fingerprint Matching Using Hough Transform," presented at the 18th Brazilian Symposium on Computer Graphics and Image Processing, 2005.

[18] X. Xie, F. Su, and A. Cai, "Ridge-Based Fingerprint Recognition," *Lecture Notes in Computer Science, vol. 3832*, Springer, pp. 273-279, 2005.

[19] G. Bebis, T. Deaconu, and M. Georgiopoulos, "Fingerprint identification using Delaunay Triangulation," *Proc. International Conference on Information Intelligence and Systems*, pp. 452-459, 1999.

[20] B. Bhanu and X. Tan, "Fingerprint Indexing Based on Novel Features of Minutiae Triplets," *IEEE Trans. on Pattern Analysis and Machine Intelligence,* vol. 25, pp. 616-622, 2003.

[21] H. Deng and Q. Huo, "Minutiae Matching Based Fingerprint Verification using Delaunay Triangulation and Aligned-Edge-Guided Triangle Matching," in *Audio- and Video-Based Biometric Person Authentication*. vol. 3546, T. Kanade, A. Jain, and N. Ratha, eds., Springer Berlin / Heidelberg, pp. 357-372, 2005.

[22] G. Parziale and A. Niel, "A Fingerprint Matching using Minutiae Triangulation," in *Biometric Authentication*. vol. 3072, D. Zhang and A. K. Jain, eds., Springer Berlin / Heidelberg, 2004, pp. 1-50.

[23] C. Wang, "Delaunay Triangulation Algorithm for Fingerprint Matching," *Proc. Third International Symposium on Voronoi Diagrams in Science and Engineering*, Banff, Canada, pp. 208-216, 2006.

[24] Y. Yin, H. Zhang, and X. Yang, "A Method based on Delaunay triangulation for Fingerprint Matching," *Proc. Biometric Technology for Human Identification II* (SPIE vol. 5779), Orlando, FL, pp. 274-281, 2005.

[25] P. Li, X. Yang, Q. Su, Y. Zhang, and J. Tian, "A Novel Fingerprint Matching Algorithm using Ridge Curvature Feature," *Proc. Third International Conference on Biometrics*, Alghero, Italy, pp. 607-616, 2009.

[26] A. K. Jain and J. Feng, "Latent Fingerprint Matching," *IEEE Trans. on Pattern Analysis and Machine Intelligence,* vol. 33, pp. 88-100, 2011.

[27] Scientific Working Group on Friction Ridge Analysis Study and Technology (SWGFAST). Available: http://www.swgfast.org

[28] R. Cappelli and D. Maltoni, "On the Spatial Distribution of Fingerprint Singularities," *IEEE Trans. on Pattern Analysis and Machine Intelligence,* vol. 31, pp. 742–748, 2009.

[29] A. Ross, S. Dass, and A. Jain, "A Deformable Model for Fingerprint Matching," *Pattern Recognition,* vol. 38, pp. 95-103, 2005.

[30] C. I. Watson, P. J. Grother, D. P. Casasent, "Distortion-tolerant filter for Elastic-distorted Fingerprint Matching," *Proc. Optical Pattern Recognition XI* (SPIE, vol. 4043), pp. 166-174, 2000.

[31] D. Maltoni, D. Maio, A. K. Jain, and S. Prabhakar, *Handbook of Fingerprint Recognition*: Springer-Verlag London Limited, 2009.

[32] N. J. Short, A. L. Abbott, M. S. Hsiao, and E. A. Fox, "Extraction of Hierarchical Extended Features in Fingerprint Images," CESCA Technical Report 2010-001, Bradley Dept. of Electrical and Computer Engineering, Virginia Tech, 2010.

[33] J. Liu, Z. Huang, and K. L. Chan, "Direct Minutiae Extraction from Gray-Level Fingerprint Image by Relationship Examination," *Proc. Int. Conf. on Image Processing,* 2000.

[34] L. Hong, Y. Wan, and A. K. Jain, "Fingerprint Image Enhancement: Algorithms and Performance Evaluation," *IEEE Trans. on Pattern Analysis and Machine Intelligence,* vol. 20, pp. 777-789, 1998.

[35] P. F. Felzenszwalb and D. P. Huttenlocher, "Distance Transforms of Sampled Functions," Cornell Comp. & Inf. Sci. Technical Report TR2004-1963, 2004.

[36] A. Blake and M. Isard, "The CONDENSATION Algorithm - Conditional Density Propogation and Applications to Visual Tracking," *Advances in Neural Information Processing,* vol. 29, pp. 5-28, 1996.

[37] A. Jain, L. Hong, and R. Bolle, "On-line Fingerprint Verification," *IEEE Transactions on Pattern Analysis and Machine Intelligence,* vol. 19, pp. 302-314, 1997.

[38] M. S. Arulampalam, S. Maskell, N. Gordon, and T. Clapp, "A Tutorial on Particle Filters for Online Nonlinear/Non-Gaussian Bayesian Tracking," *IEEE Trans. Signal Proc.,* vol. 50, pp. 174-188, 2002.

[39] N. J. Short, A. L. Abbott, M. S. Hsiao, and E. A. Fox, "A Bayesian Approach to Fingerprint Minutia Localization and Quality Assessment using Adaptable Templates," *Proc. Intl. Joint Conf. on Biometrics,* 2011.

[40] C. I. Watson, M. D. Garris, E. Tabassi, C. L. Wilson, R. M. McCabe, S. Janet, and K. Ko, "User's Guide to Non-Export Controlled Distribution of NIST Biometric Image Software," NIST Report, 2004.

[41] N. K. Ratha, S. Y. Chen, and A. K. Jain, "Adaptive Flow Orientation-based Feature Extraction in Fingerprint Images," *Pattern Recognition,* vol. 28, pp. 1657-1672, 1995.

[42] K. E. Hoyle, N. J. Short, M. S. Hsiao, A. L. Abbott, and E. A. Fox, "Minutiae + Friction Ridges = Triplet-Based Features for Determining Sufficiency in Fingerprints," *Proc. 4th International Conference on Imaging for Crime Detection and Prevention (ICDP-11)*, London, UK, 2011.

[43] S. H. Park, J. P. Leidig, L. T. Li, E. A. Fox, N. J. Short, K. E. Hoyle, A. L. Abbott, and M. S. Hsiao, "Experiment and Analysis Services in a Fingerprint Digital Library for Collaborative Research," *Proc. International Conference on Theory and Practice of Digital Libraries (TPDL 2011)*, Berlin.

[44] N. P. Kozievitch, R. d. S. Torres, S. H. P. E. A. Fox, N. J. Short, A. L. Abbott, S. Misra, and M. S. Hsiao, "Rethinking Fingerprint Evidence through Integration of Very Large Digital Libraries," *Proc. Third Workshop on Very Large Digital Libraries (VLDL2010)*, Glasgow, Scotland, 2010.

[45] C. I. Watson, M. D. Garris, E. Tabassi, C. L. Wilson, R. M. McCabe, S. Janet, and K. Ko, "User's Guide to Export Controlled Distribution of NIST Biometric Image Software," NIST Report, 2004.

[46] M. D. Garris and R. M. McCabe, " NIST Special Database 27: Fingerprint Minutiae from Latent and Matching Tenprint Images," NIST Report 6534.
Available: ftp://sequoyah.nist.gov/pub/nist_internal_reports/ir_6534.pdf

VI. Dissemination of research findings

Several publications have resulted directly from this work, and they are listed below. In addition, an internet site is currently being prepared to disseminate information related to this project. This site will contain links to the technical publications, and will provide access to databases that are being created as part of this project.

VI.1. Publications resulting from this project

The following publications have resulted from research conducted as part of this project.

- K. E. Hoyle, N. J. Short, M. S. Hsiao, A. L. Abbott, and E. A. Fox, "Minutiae + Friction Ridges = Triplet-Based Features for Determining Sufficiency in Fingerprints," *Proceedings: 4th International Conference on Imaging for Crime Detection and Prevention* (ICDP 2011), London, UK, Nov. 2011.
- N. J. Short, A. L. Abbott, M. S. Hsiao, and E. A. Fox, "Latent Fingerprint Segmentation using Ridge Template Correlation," *Proceedings: 4th International Conference on Imaging for Crime Detection and Prevention* (ICDP 2011), London, UK, Nov. 2011.
- N. J. Short, A. L. Abbott, M. S. Hsiao, and E. A. Fox, "A Bayesian Approach to Fingerprint Minutia Localization and Quality Assessment using Adaptable Templates," *Proceedings: International Joint Conference on Biometrics* (IJCB 2011), Arlington, VA, Oct. 2011.
- S. H. Park, J. P. Leidig, L. T. Li, E. A. Fox, N. J. Short, K. E. Hoyle, A. L. Abbott, and M. S. Hsiao, "Experiment and Analysis Services in a Fingerprint Digital Library for Collaborative Research," *Proceedings: International Conference on Theory and Practice of Digital Libraries* (TPDL 2011), Berlin, Sept. 2011. Also in *Lecture Notes in Computer Science* (LNCS), vol. 6966, Research and Advanced Technology for Digital Libraries, pp. 179-191, 2011.
- N. P. Kozievitch, R. da Silva Torres, S. H. Park, E. A. Fox, N. J. Short, A. L. Abbott, S. Misra, and M. S. Hsiao, "Rethinking Fingerprint Evidence through Integration of Very Large Digital Libraries," *Proceedings: Third Workshop on Very Large Digital Libraries* (VLDL2010), in conjunction with the 14th European Conference on Research and Advanced Technology for Digital Libraries (ECDL2010), Glasgow, Scotland, Sept. 2010, 8 pages.

VI.2. Invited presentations

The investigators have delivered the following invited presentations that are related to this project.

- M. S. Hsiao, A. L. Abbott, E. A. Fox, R. Murch, B. Budowle, N. J. Short, S. Misra, N. P. Kozievitch, and S. H. Park, "Toward a Quantitative Basis for Sufficiency of Friction Ridge Pattern Detail," oral presentation at Impression and Pattern Evidence Symposium, Clearwater Beach, FL, Aug. 2010.
- L. Abbott, M. S. Hsiao, E. A. Fox, R. Murch, B. Budowle, N. J. Short, S. Misra, N. P. Kozievitch, and S. H. Park, "Toward a Quantitative Basis for Sufficiency of Friction Ridge Pattern Detail," oral and poster presentations at 95th International Educational Conference, International Association for Identification, Spokane, WA, July 2010.
- L. Abbott, M. S. Hsiao, E. A. Fox, R. Murch, B. Budowle, N. J. Short, S. Misra, N. P. Kozievitch, and S. H. Park, "Development of a Quantitative Basis for Sufficiency in Friction Ridge Pattern Detail," presentation for NIJ Panel on Impression Evidence, NIJ Conference 2010, National Institute of Justice, Arlington, VA, June 14, 2010.

VI.3. Theses and dissertations

One M.S. thesis has been completed that is directly related to this project:

- Kevin E. Hoyle, "Minutiae triplet-based features with extended ridge information for determining sufficiency in fingerprints," M.S. Thesis, Bradley Department of Electrical and Computer Engineering, Virginia Tech, July 2011. (Available at http://addison.vt.edu/record=b2965528~S1.)

In addition, a Ph.D. dissertation and a second M.S. thesis are in preparation. These are expected to be completed within this calendar year.

VI.4. Technical reports

The following technical reports have been prepared during this project.

- N. J. Short, A. L. Abbott, M. S. Hsiao, and E. A. Fox, "Robust Feature Extraction in Fingerprint Images using Ridge Model Tracking," CESCA Technical Report, CESCA-2012-001, Bradley Dept. of Electrical and Computer Engineering, Virginia Tech, March 5, 2012. (http://www.cesca.centers.vt.edu/Research/publication/technical-reports/CESCA-2012-001.pdf)
- N. J. Short, A. L. Abbott, M. S. Hsiao, and E. A. Fox "A Bayesian Approach to Fingerprint Minutia Localization and Quality Assessment using Adaptable Templates," CESCA Technical Report, CESCA-2011-002, Bradley Dept. of Electrical and Computer Engineering, Virginia Tech, June 2, 2011. (http://www.cesca.centers.vt.edu/research/technical_report/TechReport_2011_002.pdf)
- K. E. Hoyle, N. J. Short, M. S. Hsiao, A. L. Abbott, and E. A. Fox, "Minutiae + Friction Ridges = Triplet-Based Features for Determining Sufficiency in Fingerprints," CESCA Technical Report, CESCA-2011-001, Bradley Dept. of Electrical and Computer Engineering, Virginia Tech, June 2, 2011. (http://www.cesca.centers.vt.edu/research/technical_report/fingerprint_sufficiency.pdf)
- N. J. Short, A. L. Abbott, M. S. Hsiao, and E. A. Fox "Extraction of Hierarchical Extended Features in Fingerprint Images," CESCA Technical Report, CESCA-2010-001, Bradley Dept. of Electrical and Computer Engineering, Virginia Tech, November 12, 2010. (http://www.cesca.centers.vt.edu/research/technical_report/TechReport_2010_001.pdf)